Dysfunction of exocytosis causes catecholamine hypersecretion in patient with pheochromocytoma

Sébastien Houy[1*], Laura Streit[1*], Ines Drissa[2], Marion Rame[1], Charles Decraene[1,10], Sophie Moog[1], Laurent Brunaud[3], Joël Lanoix[4], Rabie Chelbi[1,7], Florence Bihain[3], Stéphanie Lacomme[5], Sandra Lomazzi[5], Michel Vix[6], Didier Mutter[6], Eustache Paramithiotis[8], Christophe Dubessy[2,9], Nicolas Vitale[1], Stéphane Ory[1#] and Stéphane Gasman[1# §]

[1]*Centre National de la Recherche Scientifique, Université de Strasbourg, Institut des Neurosciences Cellulaires et Intégratives, F-67000 Strasbourg, FRANCE.*
[2]*Normandie Université, UNIROUEN, INSERM, Laboratoire Différenciation et Communication Neuronale et Neuroendocrine, F-76000 Rouen, FRANCE.*
[3]*Département de Chirurgie Viscérale, Métabolique et Cancérologique (CVMC), Unité médico-chirurgicale de chirurgie métabolique, endocrinienne et thyroïdienne (UMET), Unité médico-chirurgicale de chirurgie de l'obésité (UMCO), Université de Lorraine, CHRU NANCY, Hôpital Brabois adultes, F-54511 Vandœuvre-lès-Nancy, FRANCE.*
[4]*Institut de Recherche en Immunologie et en Cancérologie (IRIC), Université de Montréal, Montréal, QC H3C 3J7, Canada; Département de Médecine, Université de Montréal, Montréal, QC H3C 3J7, CANADA.*
[5]*Centre de Ressources Biologiques Lorrain, CHRU Nancy, Hôpitaux de Brabois, F-54511 Vandœuvre-lès-Nancy, FRANCE.*
[6]*NHC Strasbourg, Service de Chirurgie Digestive et Endocrinienne des Hôpitaux Universitaires de Strasbourg, Hôpital Civil, F-67000 Strasbourg, FRANCE.*
[7]*Inovarion, F-75005 Paris, FRANCE.*
[8]*CellCarta Biosciences, Inc., Montréal, Québec, CANADA H2X 3Y7.*
[9]*Normandie Université, UNIROUEN, INSERM, PRIMACEN, F-76000 Rouen, FRANCE.*
[10]*Centre National de la Recherche Scientifique, Université de Strasbourg, Laboratoire de Neurosciences Cognitives et Adaptatives , F-67000 Strasbourg, FRANCE.*

* S. Houy and L. Streit contributed equally to this paper
\# S. Ory and S. Gasman contributed equally to this paper
§ Corresponding author: Stéphane Gasman, address as above.
e-mail: gasman@inci-cnrs.unistra.fr

Running title: Secretion analysis in pheochromocytoma

Key words: calcium-regulated exocytosis, neuroendocrine secretion, pheochromocytoma, carbon fiber amperometry, mass spectrometry

Abstract

Pheochromocytoma (Pheo) is a neuroendocrine tumor that develops from chromaffin cells of the adrenal medulla, and is responsible of an excess of catecholamines secretion leading to severe clinical symptoms such as hypertension, elevated stroke risk and various cardiovascular complications. Surprisingly, hypersecretory activity of Pheo has never been explored at the cellular and molecular levels from individual tumor cells. In the present study, we have combined catecholamine secretion measurement by carbon fiber amperometry on human tumor cells directly cultured from freshly resected Pheo, with the analysis by mass spectrometry of the exocytotic proteins differentially expressed between the tumor and the matched adjacent non-tumor tissue. Catecholamine secretion recordings from individual Pheo cells obtained from most patients reveal a higher number of exocytic events per cell associated with faster kinetic parameters. Accordingly, we unravel significant tumor-associated modifications in the expression of key proteins involved in different steps of the calcium-regulated exocytic pathway. Altogether, our findings indicate that dysfunction of the calcium-regulated exocytosis at the level of individual Pheo cell is a cause of the tumor-associated hypersecretion of catecholamines.

Introduction

Through the secretion of hormones and neuropeptides, the neuroendocrine system controls many vital functions such as metabolism, blood pressure, reproduction, growth and development, stress and eating behavior, to cite only a few. Neoplasms can derive from all kinds of hormone secreting cells giving rise to a neuroendocrine tumor (NET). NETs constitute a highly heterogeneous group of neoplasm, but share a common feature in that they are often associated with a deregulation of hormone secretion, mainly hypersecretion, which can induce symptoms and major clinical complications (Zandee *et al*, 2017). Therefore, the secretory pathways and their dysfunction appear as an important issue to be considered in NETs. However, the cellular and molecular mechanisms underlying hypersecretory activity of NETs remain poorly known.

In neuroendocrine cells, hormones and neuropeptides are stored in large dense core vesicles (secretory granules) and are secreted through calcium-regulated exocytosis, a process that has been intensively studied for decades (Anantharam & Kreutzberger, 2019). It involves several tightly regulated trafficking steps including the recruitment of secretory granules to the cell periphery, their docking to exocytic sites of the plasma membrane, their priming and finally the fusion between the secretory granule membrane and the plasma membrane leading to the release of the intra-granular content (Burgoyne & Morgan, 2003; Lang & Jahn, 2008). Chromaffin cells of the adrenal medulla, which store and then secrete catecholamines into the blood stream, have been widely used by us and others as an experimental model to uncover the molecular mechanisms controlling calcium-regulated exocytosis (Bader *et al*, 2002; Gasman & Vitale, 2017; Malacombe *et al*, 2006).

The NETs deriving from chromaffin cells of the adrenal medulla are called pheochromocytomas (Pheo) (Lenders *et al*, 2020). Most of the Pheos are responsible for catecholamine hypersecretion leading to clinical symptoms such as permanent or paroxysmal hypertension or to cardiovascular complications including myocarditis, Takotsubo syndrome and various forms of cardiomyopathies (Lenders *et al.*, 2020; Pappachan *et al*, 2018; Pourian *et al*, 2015; Zhang *et al*, 2017). The reason for this excess of secretion is currently not known. Among the likely possibilities are an anarchic proliferation of secretory cells or an intensification of the secretory capacity at the single cell level. We therefore attempted to investigate the cellular mechanisms responsible for a possible specific secretion dysfunction in Pheo by performing carbon fiber amperometry on primary culture of human Pheo cells. This technique allows the precise measurement of individual exocytotic event dynamics in real time and in single cells (Fathali & Cans, 2018; Mosharov & Sulzer, 2005). Combined with the detection in human Pheo tissue of exocytotic protein expression changes by mass spectrometry, it allowed us to reveal upregulated exocytosis at the single cell level and to identify specific steps of the exocytotic process that are dysregulated in the tumor as well as potential actors of the molecular machinery triggering hypersecretion in Pheo.

Results

Technical workflow and overall patient characteristics

This study includes two types of analyses (see technical workflow in Figure 1) performed on histologically confirmed Pheo samples from 27 distinct patients. On one side, we have analyzed the secretory activity of single tumor cells. To do so, freshly resected Pheos originating from 22 patients were placed in primary culture in order to perform real-time single cell catecholamine secretion measurement using carbon fiber amperometry (Figure 1A). On the other side, we have used quantitative mass spectrometry analysis to measure the relative differential expression of proteins involved in the exocytic pathway from 5 other Pheo tissues, which were compared to the matched patient non-tumor adrenal tissue. To conduct this proteomic analysis, two subcellular fractions enriched for exocytic proteins (the cytosolic fraction and a low-density membrane fraction containing plasma membrane, Golgi, endosomes and secretory vesicles) were isolated from the pairs of matched non-tumor and tumor frozen tissues (Figure 1B). Note that due to the low amount of human material, it is technically impossible to perform both amperometry and mass spectrometry experiments on the same samples.

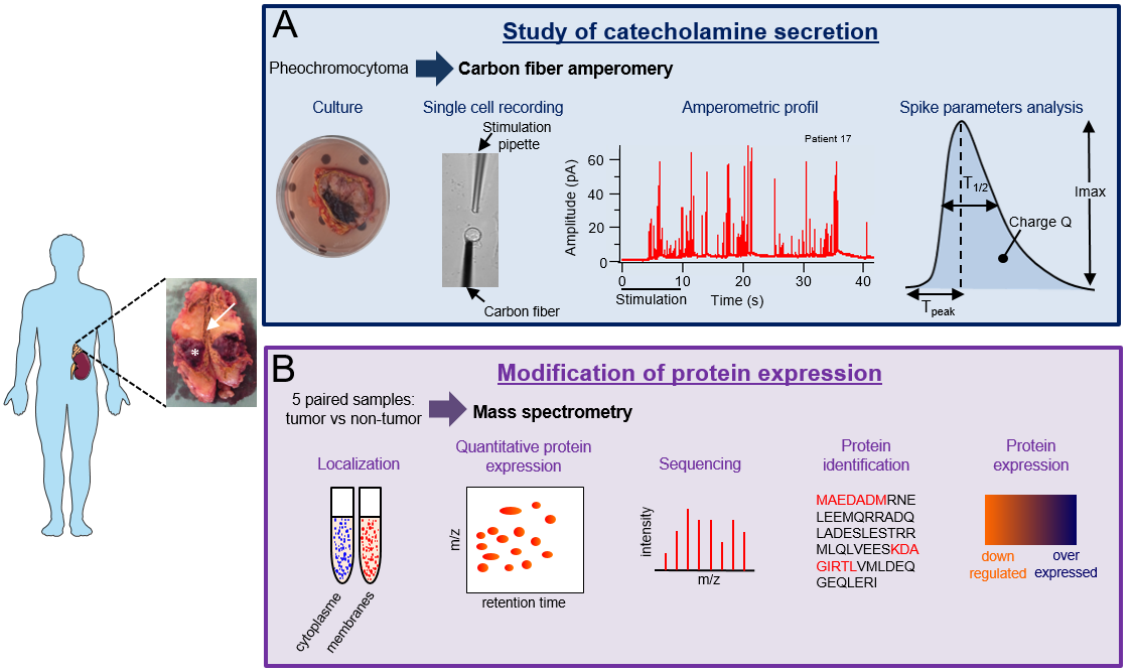

Figure 1: Technical workflow of catecholamine secretion measurement and comparative proteomic analysis of human Pheo. *A resected adrenal gland, cut in half, from a patient with Pheo is shown (asterisk). The non-tumor tissue is shown by the arrow. (A) Description of the different steps of the catecholamine secretion measurement by carbon fiber amperometry from the primary cell culture of the tumor to the amperometric spike analysis. A representative amperometric trace of a Pheo cell is illustrated. The dark bar indicates when a 100 µM nicotine solution was applied. The parameters of individual spike that were analyzed are indicated. (B) Complete protein profiling workflow of differential mass spectrometry analysis between Pheo tissue and matched non-tumor tissue.*

For patients included in the amperometric analysis, a slight predominance of male was found (59%) with a mean age of 50.5 ± 10 years at diagnosis (Table 1). Sixteen patients (73%) were diagnosed with hormonal-related symptoms whereas all of them presented abnormal hormonal secretion (100%) including adrenergic or noradrenergic phenotype in 13 (59%) and 9 (41%) cases, respectively. Seven patients (46%) out of 16 tested were diagnosed with a genetic predisposition (4 *NF1*, 1 *RET*, 1 *SDHB* and 1 *SDHD*). The mean tumor size was 4.5 cm (range 1.7-8 cm). Other biological and clinical characteristics are detailed in Table 1.

Biological and clinical characteristics of the 5 patients included for the proteomic analysis are detailed in Table 2. With a mean age of 58 ± 8 years, these 5 patients had hormonal-related symptoms at diagnosis, four of which were classified as adrenergic phenotype and one as noradrenergic phenotype. None of the patients had germline mutation (out of 3 patients tested). The mean tumor size was 5.3 cm (range 3-8 cm). Individual characteristics of the 27 patients can be found in Supplementary Table 1.

Table 1: Biological and clinical characteristics of the 22 patients from which Pheo were used for amperometric analysis.

Characteristics, *n available*	
Age at diagnosis (mean ± SD, years), *n=22*	**50.5 ± 10**
Males (%), *n=22*	**13** (59%)
Symptoms at diagnosis: *n=22*	
- Tumoral-related symptoms (%)	**4** (18%)
- Hormonal-related symptoms (%)	**16** (73%)
Hormonal hypersecretion	
- Adrenergic/noradrenergic phenotype, *n=22*	**13/9**
- Urinary MN, ULN ratio (mean ± SD), *n=19*	**9.3 ± 14**
- Urinary NMN, ULN ratio (mean ± SD), *n=19*	**7.7 ± 5.6**
- Plasma free MN, ULN ratio (mean ± SD), *n=15*	**4.5± 5.0**
- Plasma free NMN, ULN ratio (mean ± SD), *n=15*	**6.2 ± 6.1**
- Plasma CGA, ULN ratio (mean ± SD), *n=12*	**3.4 ± 2.6**
Pathology:	
- Tumor size (mean + range), *n=21*	**4.5** (1.7-8)
- Ki-67 (mean + range), *n=12*	**2.1** (1-5)
- PASS score (mean + range), *n=22*	**1.9** (0-6)
Genetics: *n=16*	
- No germline mutation (%)	**9** (56.25%)
- *NF1*	**4** (25%)
- *RET*	**1** (6.25%)
- *SDHB*	**1** (6.25%)
- *SDHD*	**1** (6.25%)

MN: metanephrine, NMN: normetanephrine, ULN: upper limit normal, CGA: chromogranin A, PASS: Pheochromocytoma of the Adrenal Gland Scaled Score, NF1: Neurofibromatosis type 1, RET: Rearranged during transfection, SDHB: Succinate dehydrogenase B, SDHD: Succinate dehydrogenase D.

Table 2: Biological and clinical characteristics of the 5 patients from which Pheo were used for proteomic analysis

Characteristics, *n available*	
Age at diagnosis (mean ± SD, years), *n=5*	**58 ± 8**
Males (%), *n=5*	**2** (40%)
Symptoms at diagnosis: *n=5*	
- Tumoral-related symptoms (%)	**1** (20%)
- Hormonal-related symptoms (%)	**5** (100%)
Hormonal hypersecretion	
- Adrenergic/noradrenergic phenotype *n=5*	**4/1**
- Urinary MN, ULN ratio (mean ± SD), *n=4*	**3.7 ± 4.2**
- Urinary NMN, ULN ratio (mean ± SD), *n=4*	**6.8 ± 8**
- Plasma free MN, ULN ratio (mean ± SD), *n=2*	**3.0 ± 2.8**
- Plasma free NMN, ULN ratio (mean ± SD), *n=2*	**3.0 ± 2.8**
- Plasma CGA, ULN ratio (mean ± SD), *n=2*	**4.7 ± 2.9**
Pathology:	
- Tumor size, cm (mean + range), *n=5*	**5.3** (3-8)
- Ki-67, % (mean + range), *n=3*	**3.3** (1-7)
- PASS score (mean + range), *n=3*	**3** (0-9)
Genetics: *n=3*	
- No germline mutation (%)	**3** (100%)

MN: metanephrine, NMN: normetanephrine, ULN: upper limit normal, CGA: chromogranin A, PASS: Pheochromocytoma of the Adrenal Gland Scaled Score.

Analysis of catecholamine secretion in human pheochromocytoma by carbon fiber amperometry

A representative amperometric trace recorded from a human Pheo cell is illustrated in Figure 1A. Each individual spike represents a single granule fusion event and is composed of a rapid rise of the electrode current corresponding to the oxidation of catecholamines quickly released at high concentration through the fusion pore as it dilates. The spike rise is then followed by a slower decay representing a decreased of the catecholamine flux through the pore as the granule empties. In addition to the quantification of number of events per cell, the analysis of individual amperometric spikes provides valuable dynamic information on the exocytic process. Hence, the surface area or quantal size (Q) is proportional to the amount of catecholamines released per event, the spike amplitude value (Imax) reflects the maximal flux of catecholamines, whereas the half-width ($T_{1/2}$), and the time to peak (T_{peak}) reflect the duration of the exocytotic event and the kinetics of the fusion pore expansion, respectively (Figure 1A).

Primary culture of human Pheo cells is rather efficient as most attempts were successful. However, culturing non-tumor chromaffin cells taken outside the tumor zone sample appeared

trickier and failed most of the time for unidentified reasons. Nevertheless, we were able to obtain 4 different cultures of non-tumor cells that could be used for amperometric recordings. Therefore, we have compared the distribution of the amperometric parameters of each of the 22 patients individually with the mean values calculated from these 4 non-tumor samples. All the amperometric parameters are detailed in Table 3. The major change concerns the total number of spikes. Indeed, among the 22 patients, 16 (73 %) exhibit a significant increase of the number of spikes (11 patients with an increase up to 2 fold and 5 patients with an increase above 2 and up to 3.4 fold; Figure 2). Hence these data suggest that one of the main causes of tumor-associated catecholamine hypersecretion could be an increase of the number of exocytic events.

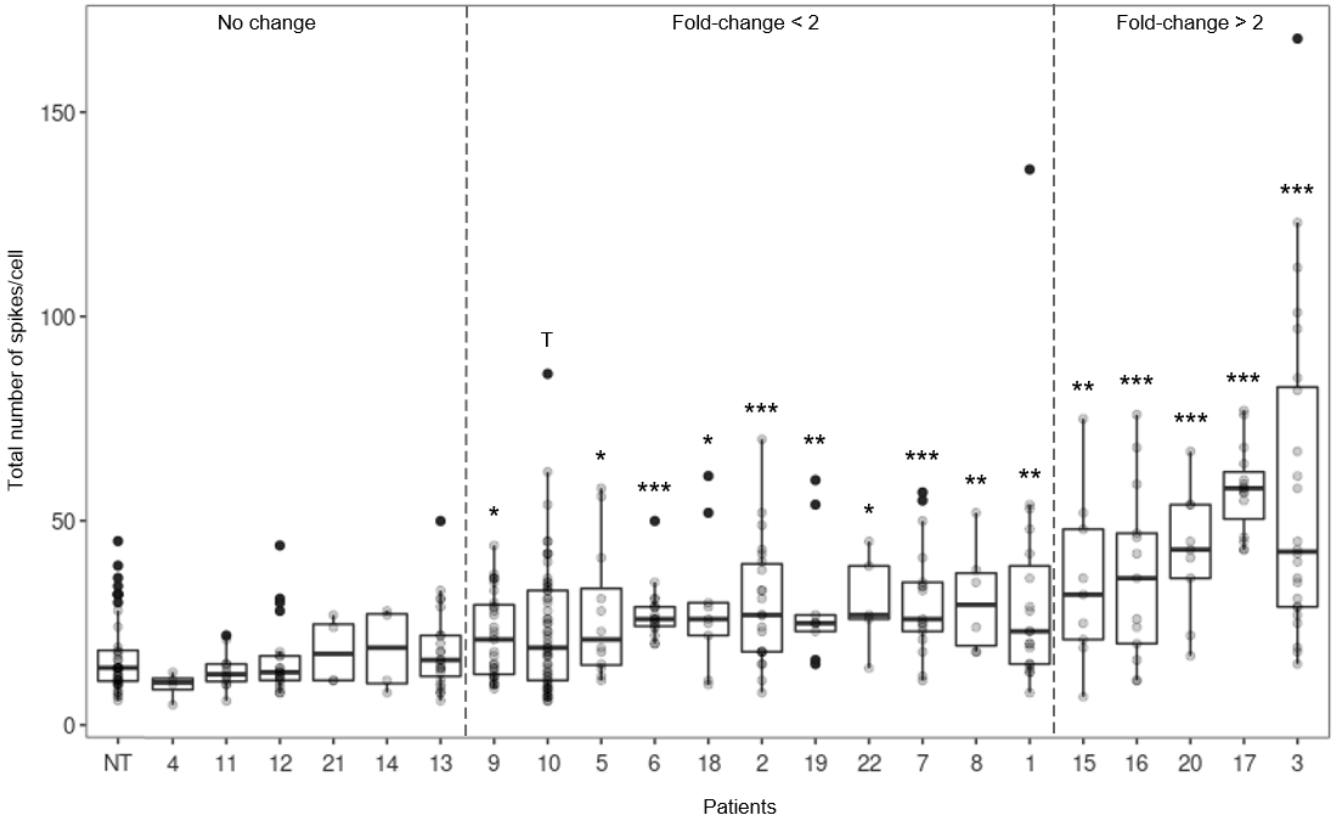

Figure 2: Analysis of catecholamine secretion events in Pheo cells from each patient by carbon fiber amperometry. *Box- and-whisker diagrams illustrating the distribution of the number of amperometric spikes per cell for non-tumor cells (NT) and for cells from each patient with Pheo. Patients are classified according to the increasing effect of the number of spikes compared to non-tumor cells: no significant change, fold-change < 2 and fold-change > 2;* $^{T}p=0.05$, *$p< 0.05$, **$p< 0.01$; ***$p< 0.001$ *compared to the mean of non-tumor tissue; non-paired Wilcoxon test.*

Table 3: Characteristics of amperometric spikes from 22 Pheos and 4 non-tumor tissues.

Identification	Number of cells	Total number of spikes	Total number of spikes/cell	Number of spikes	Imax (pA)	Charge (pC)	$T_{1/2}$ (ms)	T_{peak} (ms)
Non-tumor 1	19	224	11.79 ± 0.67	146	41.56 ± 2.23	2.22 ± 0.13	51.90 ± 1.14	42.21 ± 1.24
Non-tumor 2	11	164	14.91 ± 2.05	126	10.92 ± 0.81	0.92 ± 0.10	68.41 ± 3.41	29.87 ± 1.67
Non-tumor 3	8	144	18.00 ± 3.44	102	18.77 ± 2.35	0.73 ± 0.20	30.76 ± 3.94	13.50 ± 2.07
Non-tumor 4	6	214	35.67 ± 2.17	112	15.51 ± 1.65	0.97 ± 0.12	56.13 ± 4.26	28.50 ± 2.10
Patient 1	19	609	**32.05 ± 6.61 ****	469	21.34 ± 2.16	**0.90 ± 0.10 ***	**38.97 ± 2.70 *****	**16.37 ± 1.41 *****
Patient 2	22	653	**29.68 ± 3.26 *****	518	**12.45 ± 0.65 *****	**0.71 ± 0.04 *****	52.11 ± 1.69	**23.69 ± 1.03 *****
Patient 3	24	1388	**57.83 ± 8.01 *****	1032	27.85 ± 2.91	1.79 ± 0.16	**61.69 ± 2.74 ***	29.26 ± 1.42
Patient 4	4	39	9.75 ± 1.70	38	13.08 ± 3.20	0.71 ± 0.26	44.90 ± 8.53	21.05 ± 4.65
Patient 5	12	326	**27.17 ± 4.74 ***	240	**13.82 ± 0.92 ***	1.30 ± 0.11	**80.38 ± 5.65 *****	36.49 ± 2.11
Patient 6	18	499	**27.72 ± 1.60 *****	320	**45.78 ± 2.00 *****	**2.33 ± 0.10 *****	**48.34 ± 0.76 ***	40.43 ± 0.90
Patient 7	17	524	**30.82 ± 3.32 *****	408	**11.04 ± 0.58 ****	0.96 ± 0.07	**69.70 ± 3.27 ****	30.43 ± 1.43
Patient 8	6	185	**30.83 ± 5.46 ****	163	30.99 ± 4.50	2.00 ± 0.29	65.30 ± 6.54	31.31 ± 2.67
Patient 9	31	682	**22.00 ± 1.85 ***	416	**40.28 ± 1.61 *****	1.71 ± 0.08	**40.29 ± 1.13 *****	34.45 ± 1.18
Patient 10	59	1382	**23.42 ± 2.04 ^{T}**	1231	21.26 ± 1.28	1.25 ± 0.08	52.81 ± 2.19	**26.49 ± 1.06 ****
Patient 11	12	161	13.42 ± 1.31	130	17.39 ± 2.35	**0.85 ± 0.11 ***	**42.54 ± 2.76 ***	**19.00 ± 1.75 *****
Patient 12	21	345	16.43 ± 2.01	292	20.17 ± 2.71	**0.81 ± 0.10 ****	**35.45 ± 1.20 *****	**16.75 ± 0.84 *****
Patient 13	23	428	18.61 ± 2.16	353	**11.28 ± 0.81 *****	**0.68 ± 0.05 *****	52.01 ± 2.47	**25.47 ± 1.13 ****
Patient 14	4	74	18.50 ± 5.24	59	27.09 ± 5.68	1.01 ± 0.14	**35.08 ± 1.80 ***	**16.11 ± 0.79 ***
Patient 15	9	315	**35.00 ± 6.88 ****	187	**13.91 ± 1.93 ***	**0.49 ± 0.08 *****	**30.03 ± 1.99 *****	**14.59 ± 1.13 *****
Patient 16	12	482	**37.08 ± 5.96 *****	334	21.58 ± 2.30	**0.93 ± 0.14 ***	**37.39 ± 2.83 ****	**20.30 ± 3.34 ****
Patient 17	15	866	**57.73 ± 2.76 *****	400	23.72 ± 1.15	1.04 ± 0.06	**39.65 ± 0.89 *****	30.66 ± 0.84
Patient 18	9	266	**29.56 ± 5.66 ***	140	19.18 ± 1.75	1.72 ± 0.24	**79.57 ± 6.60 *****	**41.97 ± 4.35 ***
Patient 19	9	270	**30.00 ± 5.31 ****	197	**13.96 ± 1.03 ***	**0.55 ± 0.04 *****	**35.21 ± 1.19 *****	**17.32 ± 0.74 *****
Patient 20	9	379	**42.11 ± 5.25 *****	276	15.84 ± 2.19	**0.60 ± 0.10 *****	**33.53 ± 2.29 *****	**16.95 ± 1.58 *****
Patient 21	4	73	18.25 ± 4.23	59	16.29 ± 5.83	0.74 ± 0.19	45.37 ± 2.51	22.65 ± 1.94
Patient 22	5	151	**30.20 ± 5.42 ***	82	25.13 ± 5.40	1.72 ± 0.30	65.82 ± 6.82	32.50 ± 3.74

*Amperometric recordings were performed on primary culture of human Pheo cells or non-tumor cells. Cells were stimulated with 100 µM of nicotine for 10 s. The number of cells, the number of amperometric spikes per cell and the different amperometric spikes parameters are indicated. Results represent the mean ± SEM. Bold values are considered significantly different from the control conditions; $^{T}p=0.05$, *p< 0.05, **p< 0.01; ***p< 0.001 compared to the mean of non-tumor tissue; non-paired Wilcoxon test.*

To better understand which parameters are mostly driving the secretory tumor profiles and to sort out potential patient clusters, we performed a principal component analysis (PCA) using the amperometric data obtained from the 22 tumor cell cultures (Figure 3). As shown in Figure 3A, the 3 first principal components explain all the data variations (97.3%). The correlation matrix indicated that the main amperometric parameters explaining the variation of the data within the 2 first dimensions are the charge and the T_{peak} and to a lesser extend the $T_{1/2}$, parameters that are all correlated as shown by the variable projection analysis. The number of spikes per cell are less correlated and largely contributes to the third PCA dimension. Thus, it is interesting to note that the distribution of the patient samples plotted according to the first and the third component reveals a clear separation between populations with and without exocytic event increase as compared to non-tumor cells (Figure 3B). The distribution of the patient samples plotted according to the two first components forms one major cluster including most of the patients for which the two kinetic parameters, $T_{1/2}$ and T_{peak}, are significantly decreased (Figure 3C). Indeed, 14 (64%) patient's tumor cell cultures presented a significant reduction of the $T_{1/2}$ and/or T_{peak}, often accompanied (9 patients) with a reduction of the quantal size (Charge Q; Figure 4A, B and Table 3). This type of amperometric profile corresponds to exocytic events occurring with a faster kinetics compared to normal cells. Interestingly, among these 14 patient samples, 10 displayed a concomitant increase of spikes per cells (Figure 2). Only 4 patient's cultured cells (18%) displayed, on contrary, a significant increase of their $T_{1/2}$ leading, for two patients, to a reduce spike amplitude (Imax, patients 5 and 7, Figure 4C and Table 3) and accordingly to a slower release kinetics. Finally, 4 patient's cultured cells (18%) do not show significant changes in charge, $T_{1/2}$ or T_{peak} indicating that the kinetic of the secretion in unaffected (Figure 4D). Altogether, our analysis of the amperometric recordings indicate that catecholamine secretion in tumor cells from patients with Pheo often involves a high number and fast secretory events, which most likely contribute to the tumor-associated hypersecretion.

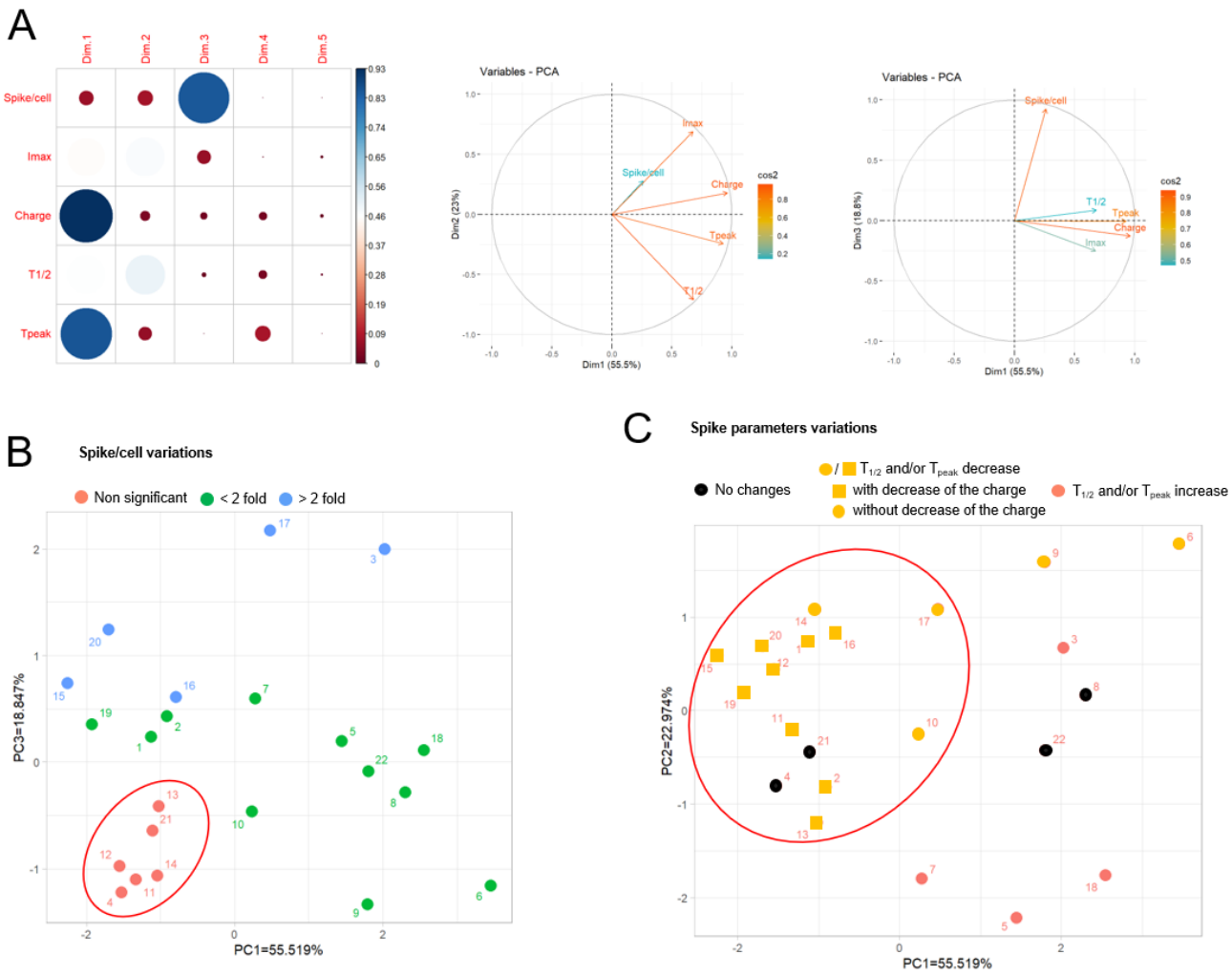

Figure 3: Principal component analysis (PCA) of amperometric spike parameters corresponding to catecholamine secretion recording on tumor cells cultured from 22 patients with Pheo. *Number of spikes/cell and spike parameters (Imax, Charge, $T_{1/2}$ and T_{peak}) were subjected to PCA. (A) Correlation matrix and variable factor maps along the PCA dimensions. The first, second and third dimension (Dim) of principal components explain 55.5%, 23.0% and 18.8% of the data variations, respectively. The spike parameters Charge and T_{peak} largely contribute to Dim 1 whereas $T_{1/2}$ and number of spikes per cell contribute to Dim 2 and 3, respectively. PCA variable vector map showing the projection of Imax, Charge, T_{peak} and $T_{1/2}$ on Dim2 (right) and Dim3 (left). The projection of each variable vector gives an indication of the relation of these variables to T_{peak} and Charge (Dim1) or spikes/cell (Dim3) (B-C) The two-dimensional representation of PC1 and PC3 (B) allowed to separate patients according to the significant variation of the number of spikes recorded per cell (red circle = no changes; green circles = fold change < 2; blue circles = fold change > 2). The two-dimensional representation of PC1 and PC2 (C) revealed a large cluster of patients for which $T_{1/2}$ and/or T_{peak} decreased (yellow squares and circles).*

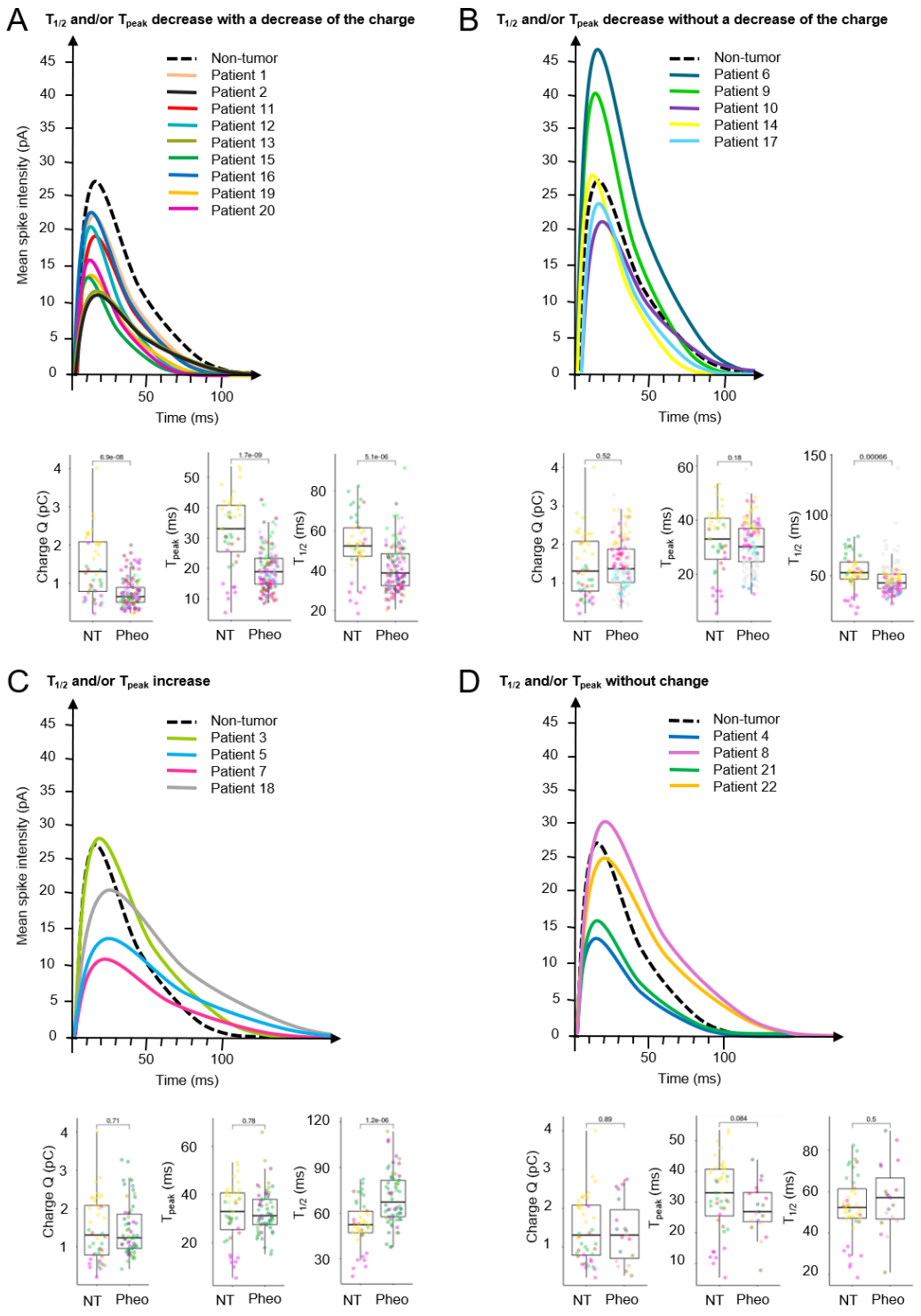

Figure 4: Analysis of amperometric spike parameters in Pheo cells from each patient. *Superimposition of the averaged spike obtained for cells of each patient and distribution of the values corresponding to the spike charge (Q), the spike rise time (T_{peak}) and the spike half-width $T_{1/2}$ are shown for the 4 different populations of patients: decrease of $T_{1/2}$ and/or T_{peak} with lower charge (A), decrease of $T_{1/2}$ and/or T_{peak} without lower charge (B), increase of $T_{1/2}$ and/or T_{peak} (C) and no significant changes of $T_{1/2}$ and/or T_{peak} (D). Box- and-whisker diagrams illustrate the distribution of each variable values pooled from all the patients belonging to the indicated secretory profile. P values are indicated and patients are color coded. All the average amperometric data are detailed in Table 3.*

Differential protein expression of the exocytic machinery in human pheochromocytoma

Since catecholamine release is altered in Pheo, we asked whether proteins of the core machinery of secretory granule exocytic process could be deregulated. To do so, we performed a mass spectrometry analysis comparing 5 pairs of human Pheo with their respective matched adjacent non-tumor tissue. To increase detection and sensitivity, we conducted the proteomic analysis on purified subcellular fractions in place of total homogenate. Two main subcellular fractions were isolated from each tissue sample, a membrane fraction enriched for organelles and vesicles derived from the exocytic pathway and a fraction enriched in cytosolic proteins. From our proteomic data set, we selected proteins from the regulated exocytosis (#BPGO:0045055) and secretory granule (#CCGO:0030141) GO terms and focused on proteins significantly up or downregulated in the tumor by comparison with the corresponding non-tumor tissue, with fold change values greater than or equal to 2. In these conditions, we identified 166 deregulated proteins: 62 proteins from the cytosolic fraction, 54 from the membrane-enriched fraction and 50 common to both fractions (Figure 5A). Supplementary Table 2 details the median value of the relative expression changes of the 5 pairs of Pheo samples for all these 166 selected proteins associated with their known function. The volcano plot in Figure 5B shows the relationship between the p-values and the fold change in expression. The unsupervised hierarchical clustering of all differentially expressed proteins in row according to the paired samples in columns, is presented in Figure 5C for the corresponding cellular compartment. Note that the expression of proteins found in common in the membranous and the cytosolic fractions varies in the same direction (Supplementary Figure 1). This specific dataset of proteins corresponding to the proteins involved in the machinery of secretory granule exocytotic process clearly differentiate, by their modulation of expressions, the Pheo samples from the non-tumor samples. The functions of the deregulated proteins linked to secretory granule exocytosis include mainly: secretory granule organization and biogenesis, hormone processing, vesicular trafficking, docking, priming, membrane fusion, actin cytoskeleton organization, and small GTPases (Supplementary Table 2 and Figure 5D). Hence, we observed that numerous secretory granules cargos, as well as different proteins involved in the control of the frequency and the dynamic of the exocytic events are up-regulated.

A

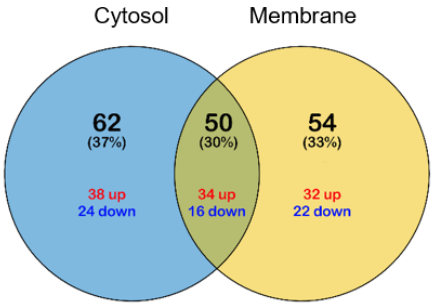

B

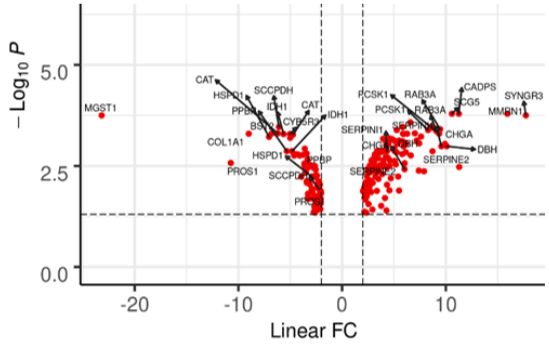

C

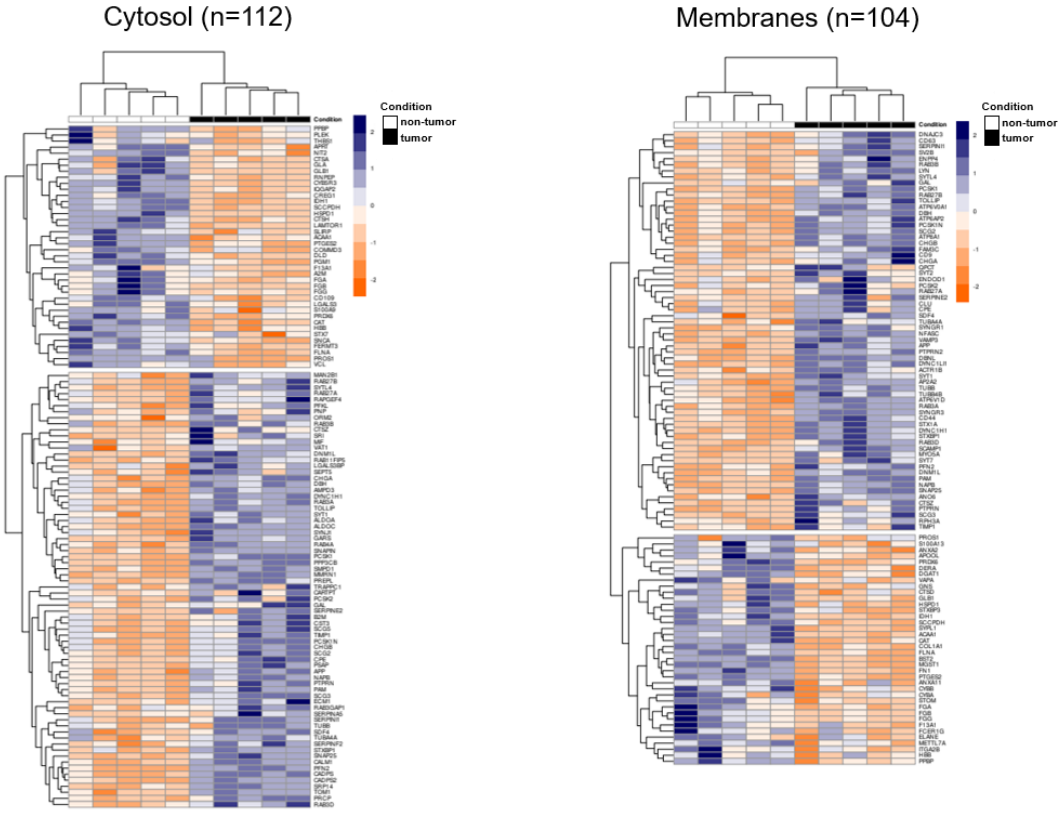

D

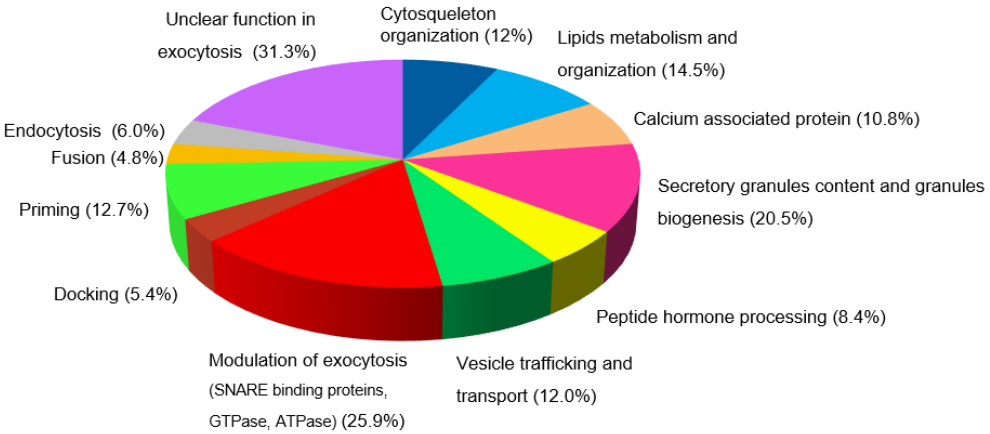

Figure 5: Identification of differentially expressed proteins involved in the exocytotic pathway in human Pheo tissue. *(A) Venn diagram showing the distribution of the differentially expressed proteins in fractions enriched in cytosolic and membrane proteins. Colors indicate up- (red) or down- (blue) regulation. (B) Volcano plot of all differentially expressed proteins between Pheo and non-tumor samples. (C) Two-way hierarchical clustering of paired samples from each patient (non-tumor in white and tumor in black) in column according to the validated cytosolic (left) and membranous (right) proteins of the data set in row. Protein expression values were z-score normalized prior to clustering using the complete-linkage method together with the Euclidean distance. Each row represents a differentially expressed protein and each column, a patient according to the tissue type. The color scale illustrates the relative level of protein expression: red, higher expression; blue, lower expression. (D) Functional enrichment analysis of identified proteins. Each differentially expressed protein selected for their potential role in calcium-regulated exocytosis (Table 4) has been classified in one or several indicated biological functions.*

To further assess the relevance of our data, we have compared our proteome dataset to a published gene expression analysis of 60 Pheo and 6 normal adrenal medulla tissues ((Lopez-Jimenez *et al*, 2010) https://www.ncbi.nlm.nih.gov/geo/query/acc.cgi?acc=GSE19422). Using this analysis, we have extracted 170 genes that belong at least to one of the 2 GO terms used in the proteomic analysis (regulated exocytosis and secretory granules) and that are significantly differentially expressed by at least two-fold between Pheo and normal adrenal tissues. Interestingly, among these 170 genes, 59 are common to our proteome dataset. As observed at the level of the protein expression changes, the hierarchical clustering of these 59 differentially expressed genes efficiently separated the tumor samples from the normal adrenal tissue (Figure 6A). Moreover, the expression of 53 of these 59 genes (90%) shows the same variation trend as the protein expression, both in the cytosol and in the membranes (Figures 6B and Supplementary Figure 2). To visualize whether the deregulated proteins identified in this comparison were highly connected to each other, we performed a protein-protein interaction (PPI) network analysis using Cytoscape ((Shannon *et al*, 2003), Figure 7). Interestingly, one major significant cluster is composed of proteins that are overexpressed both at the protein and at the gene levels (blue squares). The cluster includes proteins involved in the secretory granule composition such as various chromogranins (CHGA, CHGB, SCG2, SCG3, SCG5), in catecholamine synthesis or in hormone processing (DBH, PCSK1, PCSK2, CPE, PAM), in granule docking and fusion such as different SNAREs or SNAREs interacting proteins (SNAP25, STX1A, SYTL4, STXBP1, SYT1) and Rab GTPases (RAB3A, RAB3D, RAB27B).

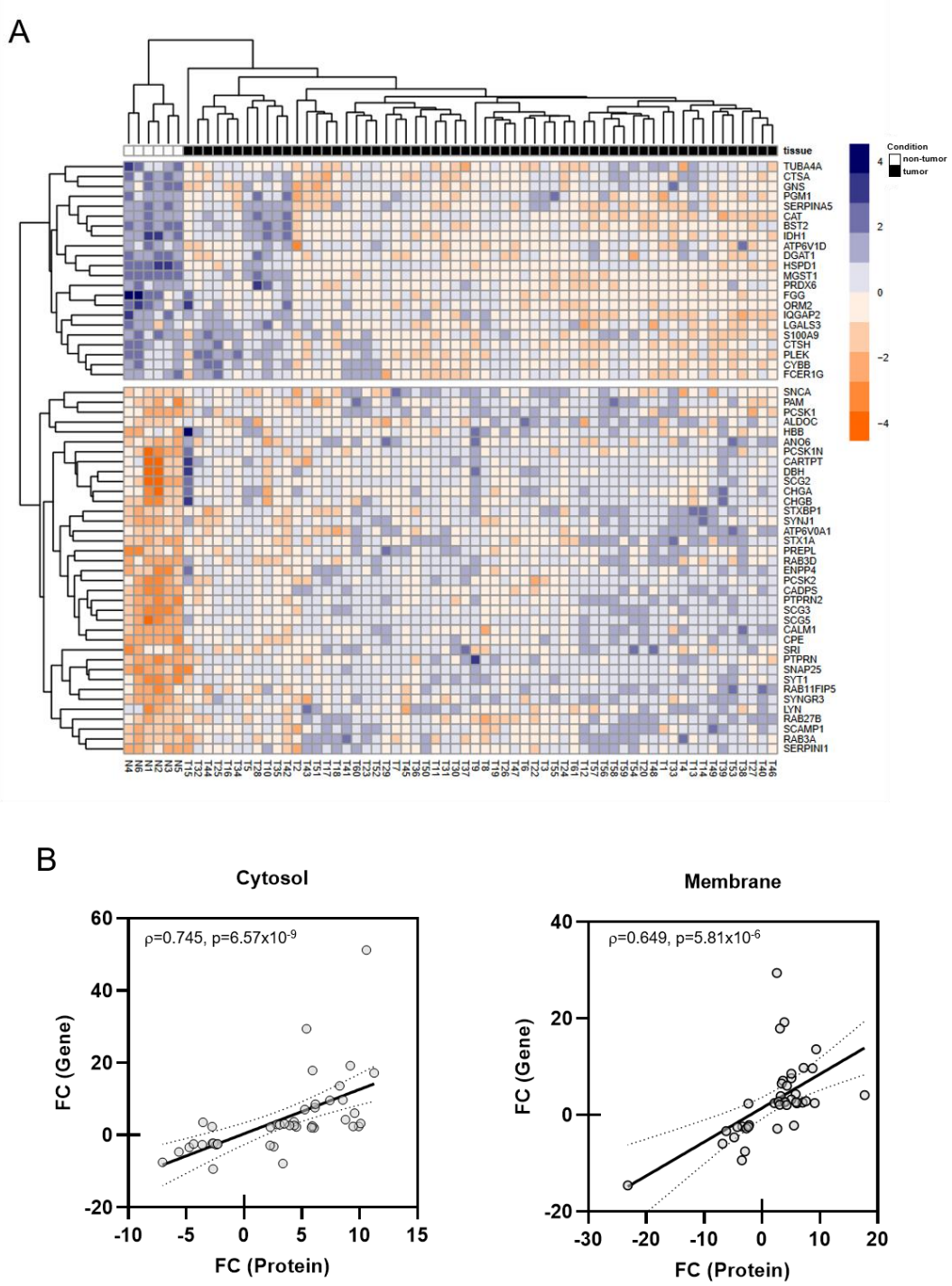

Figure 6: Comparison of the proteome dataset with a published gene expression analysis of 60 Pheo and 6 normal adrenal medulla tissues. *(A) Unsupervised hierarchical clustering of selected gene expression profiles (n=59) for 6 non-tumor adrenal medulla (in white) and 60 pheochromocytomas (in black) tissues from Lopez-Jimenez et al. (2010). The color scale illustrates the relative level of gene expression: blue, highly expressed gene; red, low expressed gene. (B) A significant positive correlation was evidenced between the fold changes (FC) in expression of genes and corresponding cytosolic or membrane proteins of the exocytosis pathway. Linear regression (solid line) and 95% confidence bands (the regions delineated by dotted lines) are shown.*

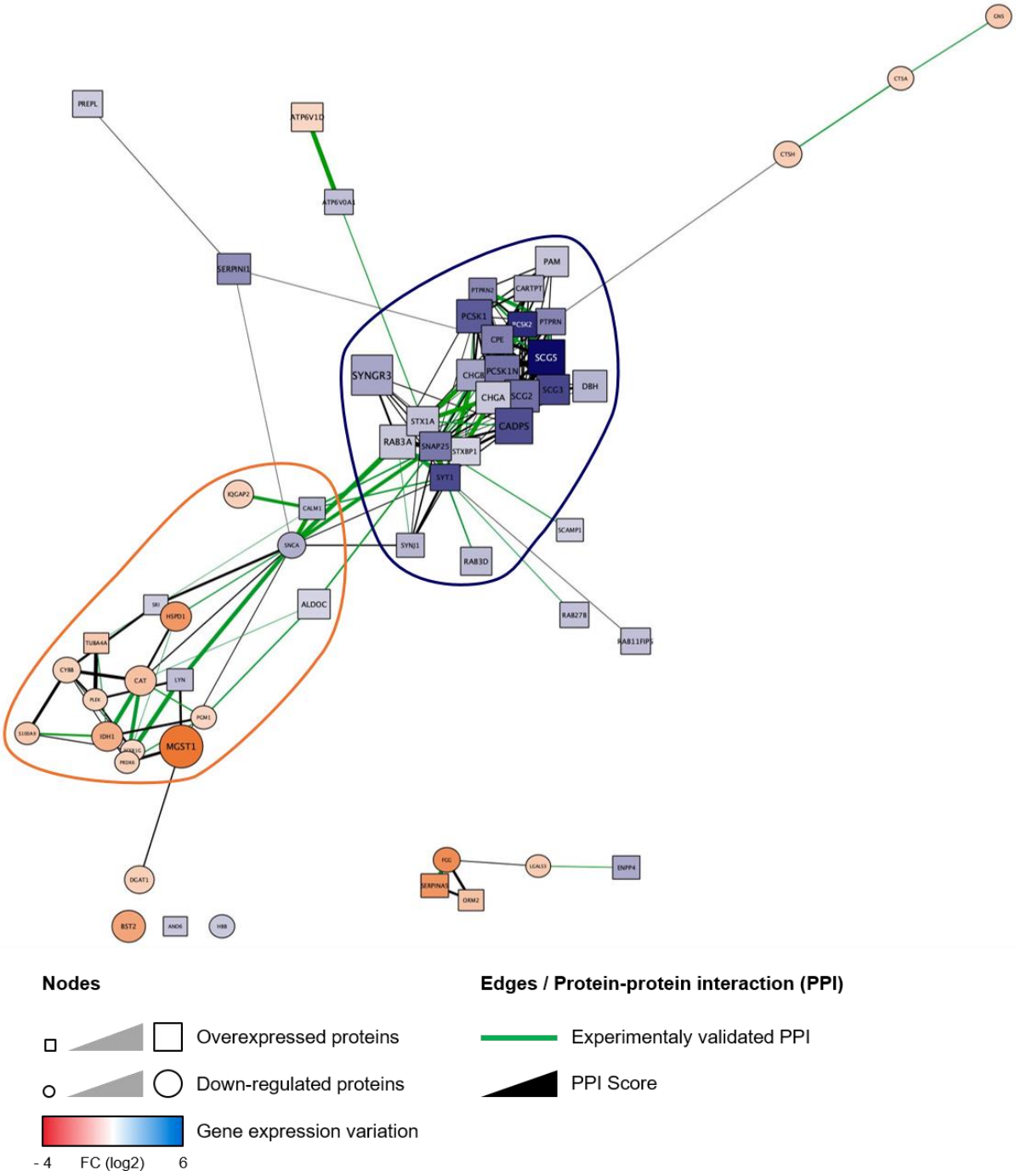

Figure 7: Protein-protein interaction (PPI) network analysis of the exocytic proteins modulated in Pheo at the transcriptomic and protein level. *The PPI network was generated using Cytoscape. Overexpressed and downregulated proteins are represented by square and round nodes, respectively and the level of protein expression is proportional to their size whereas the mRNA expression variation is color coded as indicated. Therefore blue squares and red circles represent candidate for which both protein and mRNA are overexpressed or downregulated, respectively. The 2 first clusters identified by the CytoCluster plugin are outlined in blue ($p=2.74x10^{-9}$) and red ($p=3.65x10^{-6}$). Note that the variation observed at the protein and mRNA level goes in the same direction for 53 proteins out of 59 (90%).*

Finally, to further validate our dataset, we analyzed the global expression change of some key overexpressed proteins present in the main exocytic cluster identified with Cytoscape. To do so, we performed a multiplexed MRM MS assay in total protein homogenates prepared from another independent cohort of 25 pairs of human Pheo and their matched non-tumor tissue (Croise *et al*, 2016). As MRM is a targeted MS approach that uses synthetic peptide reference standards, it is used to confirm and quantify the presence of proteins of interest on smaller amounts of sample with high sensitivity, which eliminates the need for fractionation (Keshishian *et al*, 2007). As observed for the subcellular fractions, using MRM MS we found that the expression of every protein identified in the PPI analysis was also significantly increased in Pheos compared with the matched adjacent non-tumor adrenal tissue (Figure 8).

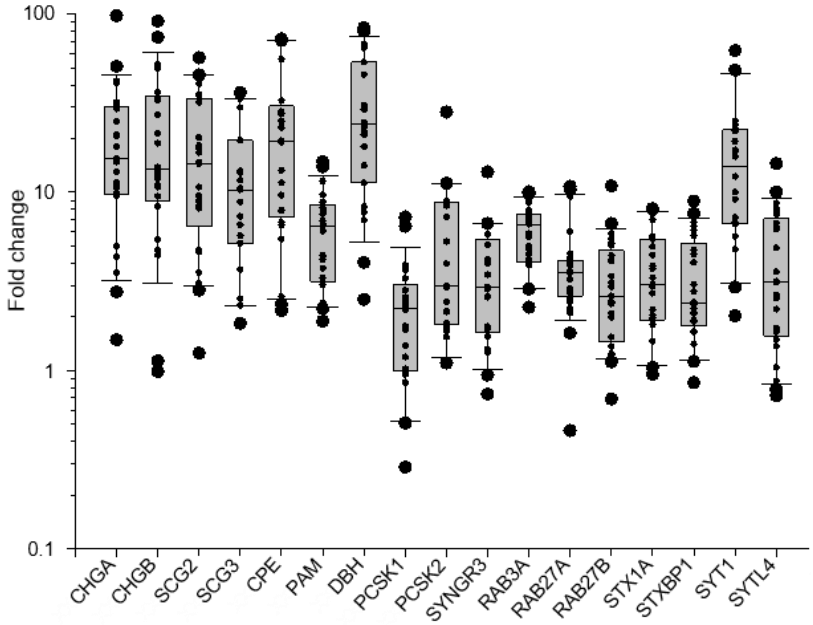

Figure 8: Global variation of key exocytic proteins expression in human Pheo tissue. *Expression variation of the indicated proteins was quantified at the protein level by MRM-MS in 25 pairs of human Pheo normalized to their matched adjacent non-tumor tissue. Box- and-whisker diagrams illustrate the distribution of protein expression fold change (FC) for the 25 Pheos.*

Discussion

Dysfunction of hormones and neuropeptides secretion in NETs is a serious health issue. Patients with midgut primary carcinoids have increased serotonin and metabolite secretion, corresponding to higher metastatic tumor burdens (Onaitis *et al*, 2000). Hypersecretion of serotonin by carcinoid tumor from the gastro-intestinal tract can trigger carcinoid syndrome, which is associated with severe consequences such as flushing, diarrhea, bronchoconstriction and cardiac valvular disease (Onaitis *et al.*, 2000). Acromegaly often result from excessive secretion of growth hormone by pituitary adenoma (Dineen *et al*, 2017). Excessive level of circulating catecholamines in patients with Pheo can trigger life-threatening medical problems such as cardiopathy and stroke (Y-Hassan & Falhammar, 2020; Zhang *et al.*, 2017). Moreover, enhanced secretory activity of NET cells may develop over time with negative impact on prognosis. For example, silent pituitary adenoma can evolve into an active secreting adenoma whereas non-functional pancreatic tumors can become hormonally active, hence turning to a more aggressive tumor phenotype (Brown *et al*, 2006; Daems *et al*, 2009; Juhlin *et al*, 2019). Small cell lung cancer (SCLC) is a high-grade malignant cancer due to the progressive neuroendocrine nature of SCLC cells that secrete a variety of neuropeptides, together with growth factors that all dramatically accelerate the invasive growth by their autocrine action (Cuttitta *et al*, 1985; Song *et al*, 2003). Altogether, these few examples taken from a longer list clearly reveals that dysfunction of the secretory pathways in NETs can lead to severe clinical complications and can also impact the tumor development and prognosis. Today, a clear unmet need is to identify the cellular and molecular mechanisms triggering hypersecretory activity in NETs.

The aim of the present study was thus to uncover part of the mechanisms triggering catecholamine hypersecretion in human Pheo cells. To do so, we have used carbon fiber amperometry recordings to analyze catecholamine secretion on individual tumor cells cultured directly from freshly resected human Pheos. In parallel, we have analyzed the expression level of various proteins involved in calcium-regulated exocytosis by differential mass spectrometry methods applied on human Pheo tissues.

At the cellular level, several hypotheses which may not be mutually exclusive could explain the hypersecretory phenotype of Pheo: i) a leakage of catecholamines through the constitutive secretory pathway, ii) a global increase in the quantity of catecholamines in the secretory granules, iii) a simple mass effect, as the number of cells increases within the tumor and iv) a dysfunction of the calcium-regulated secretory pathway. Interestingly, our amperometric analysis has allowed us to identify the later possibility as a likely cause of this phenomenon. First, leakage of catecholamines in resting tumor cells does probably not occur as we never observed any spontaneous amperometric spike in the absence of cell stimulation (data not shown). Second, an increase of catecholamines in the secretory granules is rather unlikely since in most cases, quantal size of individual secretory events was not increased. Third, we showed that the number of exocytic events is significantly increased in single tumor

chromaffin cells compared to non-tumor cells indicating that the cell proliferation within the tumor cannot be responsible alone for the hypersecretion phenotype. Moreover, by analyzing the spike kinetics, we have also observed that, for many patients, exocytic events tend to be faster. Altogether, our data clearly demonstrated that the regulation of calcium-regulated exocytosis is highly perturbed in tumor cells. To our knowledge, this is the first report analysing the catecholamine secretion using carbon fiber amperometry recording directly performed on human tumor cells from freshly resected pheochromocytomas.

The specific step of the exocytic pathway and which proteins might be involved in this amplified secretory activity remain to be explored in details. However, a significant increase in spike frequency can be consistent with an increase in efficiency of the different steps upstream of the fusion process including recruitment, docking and priming or with a greater calcium sensitivity of the exocytosis machinery. Faster kinetics of the exocytotic events might also reflect a direct effect on the fusion process. Through the differential mass spectrometry analysis, we have identified several proteins involved in the regulation of these various step of exocytosis, that are significantly over-expressed in the tumor tissue compared to the non-tumor tissue. Among them, some are known to affect the amperometric spike frequency and/or the kinetics of the spikes when their expression changes in chromaffin cells. This is the case for example of SNARE proteins (SNAP25, Syntaxin1), as well as for proteins regulating the SNARE complex (Synaptotagmin-1 and -7) or for the actin cytoskeleton organization (Rab27A or Annexin-A2) (Desnos *et al*, 2003; Fang *et al*, 2008; Gabel *et al*, 2015; Tawfik *et al*, 2021). Of note, among the core exocytotic machinery the calcium sensor synaptotagmin-1 was found to be among the most overexpressed in tumor cells (Figure 8), which could lead to an increase in calcium sensitivity and probability of release. Finally, it must be mentioned that at this stage, we cannot rule out an increase of the number of secretory granules in tumor cells as various specific soluble cargos of secretory granules, like different chromogranins or enzymes involved in hormone processing, were also found to be overexpressed. These observations are in line with previous reports indicating that chromogranins or chromogranin-derived peptides are highly expressed in Pheo (Guerin *et al*, 2010), and often found at higher levels in human fluids, which makes some of the proteins identified in our screen biomarker candidates.

To conclude, we have reported here that calcium-regulated exocytosis is deregulated in human Pheo cells and we have described tumor-associated expression changes of various key players of the exocytic pathway. The next challenge will be to understand how exactly these changes lead to the hypersecretion of catecholamines by the tumor. Moreover, a key unmet need is to find molecules able to prevent the catecholamine hypersecretion directly from the tumor cells. Of note, we have recently identified the somatostatin analog pasireotide (SOM230) as a *bona fide* inhibitor of Pheo hypersecretion (Streit *et al*, 2021), but the probable mechanism of action of this drug involves an inhibition of the cholinergic stimulation, which may prove to affect the activity of a large variety of secretory cells possessing nicotinic receptors. There is therefore a need to correct hypersecretion by identifying specific alterations in the secretory machinery whose potential candidates are identified in this study.

Material and methods

Subjects and samples

The medical files of patients with Pheo in 2 French centers (CHRU, Nancy and NHC, Strasbourg) between 2013 and 2020 were retrospectively reviewed. We collected initial diagnosis, including a clinical examination looking for hormonal-related symptoms and biological analysis. As recommended by the Endocrine Society clinical practice guideline published in 2014 (Lenders *et al*, 2014), Pheo genetic testing was proposed to identify germline mutations in the major susceptibility genes (SDHB, SDHC, SDHD, VHL, NF1, RET, TMEM127, MAX) using Sanger sequencing and multiplex ligation-dependent probe amplification (MLPA). Then, as recommended in the consensus statement published in 2017 (Group *et al*, 2017), next-generation-sequencing (NGS)-based diagnostic was carried out for more recent patients. Biological analysis comprised the measurement of metanephrine (MN) and normetanephrine (NMN) levels (in urine and/or plasma). When available, chromogranin A (CGA) measurements were also registered. Levels of free MN, NMN and CGA in plasma, as well as urinary levels of MN and NMN are presented as ratios normalized by the upper limits of normal (ULN). Plasma and urinary MN or NMN levels reaching two-fold the upper limit of the normal range and/or CGA exceeding the upper limit of the normal range was defined as the threshold of abnormal hormonal secretion (Lenders *et al.*, 2020). The ULN of free MN and NM were 4.05 and 9.8 nmol/L in plasma and 1625 and 2620 nmol/24 h in urine, respectively. The upper reference limit for CGA was 100 mg/L. Catecholamine-producing phenotype of Pheo were categorized as previously described (Eisenhofer *et al*, 2005): adrenergic (AD) phenotype, when MN content exceeded 10% of the combined MN and NMN contents, or noradrenergic (NAD) phenotype when MN content remained below 10% of the combined MN and NMN contents. Pathological evaluation was reviewed, including tumor size, Ki-67 result and the PASS (Pheochromocytoma of the Adrenal Gland Scaled Score) as previously described (Thompson, 2002). Biological and clinical characteristics are summarized in Tables 1 and 2 whereas details per patient are described in Supplementary Table 1.

Primary culture of human pheochromocytoma cells

Human tumor cells were cultured from freshly resected Pheo following surgery (Moog *et al*, 2018). In the operating room and immediately after the resection, the adrenal gland was cut longitudinally in two parts. Roughly a 1 cm^3 piece of tumor tissue was dissected and immediately plunged into ice cold transport medium (Ca^{2+}- and Mg^{2+}-free Hank's Balanced Salt Solution (CMF HBSS, Sigma) supplemented with 0.2% Fetal Bovine Serum (FBS, Gibco) and 1% penicillin/streptomycin (Sigma) or MACS Medium Tissue Storage solution (Miltenyi Biotec). Up to 3 hours after resection, the tumor sample was minced into 1 mm^3 pieces in a dish containing CMF HBSS. Chunks were collected, centrifuged at 250 g for 5 min at room temperature and the pellet resuspended in 15 mL of complete medium (RPMI 1640 GlutaMAX™ (Gibco), 15% FBS, 1% penicillin/streptomycin). Red blood cells, debris and fat were separated from minced tissue by sedimentation for 15 min at room temperature. The supernatant was removed and 15 mL of complete medium were added to the pellet before centrifugation at 250 g for 5 min. Tumor pieces were resuspended in HBSS (in 10 times the tissue volume), containing 1.5 mg/mL of collagenase B (Roche) and 1 mg/mL of the protease

dispase II (Gibco) and gently rocked for 45 min at 37°C. 5 min before the end of protease digestion, 0.1 mg/mL DNase I (Roche) was added to remove potential DNA clumps. Samples were left for a few minutes to sediment at room temperature and supernatant recovered (fraction 1). The pellet was resuspended in 5 mL of CMF HBSS and triturated for a couple of minutes to dislodge tumor cells from chunks. The remaining pieces were left few minutes to sediment and the supernatant recovered (fraction 2). Both fractions were centrifuged at 800 g for 5 min at room temperature. Cell pellets were resuspended in 2 mL of CMF HBSS. 4 mL of Red Blood Cell Lysis Buffer (Roche) were added before being gently rocked for 10 min at room temperature. The fractions were centrifuged at 500 g for 5 min and resuspended into complete medium. Cell viability and density were estimated under a microscope and 300 µL of cell suspension were seeded into type I collagen (Corning)-coated 35 mm dishes (MatTek). Cells were left to adhere overnight at 37°C in an incubator with water-saturated and 5% CO_2 atmosphere. 2 mL of complete RPMI were added the following day and cells were used within two days.

Carbon fiber amperometry

Human tumor cells from freshly resected pheochromocytoma were washed with Locke's solution (140 mM NaCl, 4.7 mM KCl, 2.5 mM $CaCl_2$, 1.2 mM KH_2PO_4, 1.2 mM $MgSO_4$, 11 mM glucose, 0.01 mM EDTA and 15 mM HEPES, pH 7.5) and processed for catecholamine release measurements by amperometry as previously described (Houy *et al*, 2015; Tanguy *et al*, 2020). A carbon fiber electrode of 5 µm diameter (ALA Scientific Instruments) was held at a potential of +650 mV compared with the reference electrode (Ag/AgCl) and approached close to one cell. Secretion of catecholamines was induced by a 10 s pressure ejection of a 100 µM nicotine (Sigma) solution from a micropipette (Femtotips®, Eppendorf) positioned 10 µm from the cell and recorded over 60 s. The amperometric recordings were performed with an AMU130 amplifier (Radiometer Analytical), calibrated at 5 kHz, and digitally low-pass filtered at 1 kHz. Analysis of the amperometric recordings was performed as previously described with a macro (laboratory of Dr. R. Borges; http://webpages.ull.es/users/rborges/) written for Igor software (WaveMetrics), allowing automatic spike detection and extraction of spike parameters (Segura *et al*, 2000). The spike parameters analysis was restricted to spikes with amplitudes higher than 5 pA, which were considered as exocytic events. All spikes identified by the program were visually inspected. Overlapping spikes and spikes with aberrant shapes were discarded for parameters analysis. Quantal size (spike charge, Q) of each individual spike was measured by calculating the spike area above the baseline. Spike area is defined as the time integral of each transient current, Imax as the height of each spike, half-width as the width of each spike at half its height ($T_{1/2}$) and T_{peak} as the spike rise time (Figure 1A).

Tissue fractionation

Frozen tumor and matched non-tumor adjacent tissues were cut into small pieces (~10 mm^3), and 3 mL of homogenization buffer (0.25 M sucrose, 10 mM Tris pH 7.4, 100 units/mL of DNase I, 5 mM $MgCl_2$, Complete protease inhibitor EDTA-free cocktail) was added per tissue sample, homogenized twice for 10 s and one time for 20 s using a polytron set at speed 4.0. Homogenates were filtered through a 180 µm nylon and brought to 3 mL with the homogenization buffer, if necessary. Light membranes were obtained by isopycnic

centrifugation using discontinuous sucrose gradients in which samples brought to 1.4 M sucrose were layered by 1.2 M and 0.8 M sucrose. After centrifugation at 155,000 g for 2 hours at 4°C, the light membrane fraction located at the 0.8 M to 1.2 M sucrose interface was collected, snap-frozen in liquid nitrogen and stored at -80°C. The light membrane fraction is enriched with plasma membrane, Golgi, endosomes and secretory pathway associated membranes. The cytosol fractions were obtained by centrifuging 200 µL of crude homogenates at 150,000 g for 1 hour at 4°C. The supernatant was collected, snap-frozen and stored at -80°C.
The amounts of protein were determined using the bicinchoninic acid (BCA) assay according to the manufacturer's instructions (Pierce).

Mass spectrometry analysis

30 µg of samples (homogenates, cytosol or light membranes) was incubated in a denaturing buffer at final concentration of 7 M urea, 175 mM NH_4HCO_3, 8.75% v/v acetonitrile and incubated for 30 min at room temperature. Samples were then diluted to 1 M urea with water and digested with trypsin (Promega) overnight at 37°C at a ratio of 1 µg of trypsin per 10 µg of protein for homogenate and cytosol samples while for light membranes, the ratio was set at 1 µg of trypsin per 25 µg of proteins. Samples were reduced with 10 mM tris(2-carboxyethyl)phosphine (final concentration), incubated for 30 min at room temperature and then acidified to 0.5 M HCl. The samples were desalted using C18 96-well plates (3M Empore). The C18 eluates from homogenate samples were evaporated and stored at 4°C prior to MS analysis. The C18 eluates from light membrane and cytosol samples were collected in injection plates for strong cation exchange (SCX), dried by vacuum evaporation and stored at -20°C.
To fractionate peptides by SCX chromatography, samples were solubilized with reconstitution buffer (0.2% v/v formic acid, 10% v/v acetonitrile for light membrane samples; 20 mM K_2HPO_4, 25% v/v acetonitrile for cytosol samples) and loaded on an SCX column. Three fractions were collected following elution using a salt gradient. At the end of each SCX fractionation batch, the collected fractions were stored at -80°C. Once the SCX fractionation was completed, the fractions were freeze-dried and then desalted. The eluates were divided equally into two 96-well plates; one plate for LC-MS/MS analysis and the other plate as a back-up. All plates were vacuum evaporated and stored at -20°C until analysis by LC-MS/MS. Samples were resuspended in 92.5/7.5 water/ACN+0.2% formic acid and analyzed by LC-MS/MS on a nanoAcquity UPLC (Waters) coupled to a Q-Exactive mass spectrometer (Thermo). Survey (LC-MS) and tandem mass spectrometry scans (MS/MS) were acquired in the same run. The resolution for the MS and MS/MS scans were 70,000 and 17,500, respectively. Peptide separation was achieved using a Waters nanoAcquity Symmetry UPLC Trap column (180 µm x 20 mm, 5 µm particle size) and a Waters nanoAcquity UPLC BEH300 analytical column (150 µm x 100 mm, 1.7 µm particle size). The mobile phases were (A) 0.2% formic acid in water and (B) 0.2% formic acid in acetonitrile. For each sample approximately 3.6 µg was loaded onto the trap column for 3 min at a flow rate of 10 µL/min. Peptides were separated using a linear gradient (92.5% A to 84% A) for 26 min, followed by (84% A to 75% A) for 14 min and a wash at 60% B for 2 min. The flow rate was 1.8 µL/min. Protein identification was accomplished using data acquired by LC-MS/MS. The MS/MS spectra were matched to the corresponding peptide sequences found in the UniProt human protein database using Mascot (Matrix Science, version 2.2.06.) software.

Multiplexed multiple reaction monitoring (MRM) assay

For each of the selected proteins, five MRM-suitable peptides were selected by CellCarta's in-house MRM Peptide Selection software. If possible, peptides that were detected by mass spectrometry were prioritized. The selected peptides were synthesized by JPT Peptide Technologies (Germany). Synthesized peptides were resolubilized in 25%/75% water/DMSO (v/v), pooled and diluted with 0.2% formic acid in water to a concentration of 200 pmol/mL. This peptide mix was used to develop the MRM assay. The optimal 2 transitions (combination of peptide precursor and fragment ion mass-to-charge ratio that are monitored by the mass spectrometer) per peptide were determined using selected reaction monitoring (SRM)-triggered MS/MS on a QTRAP 5500 instrument (AB Sciex) coupled to a nanoAcquity UPLC (Waters). An SRM transition was predicted for each peptide. The detection of this transition triggered the acquisition of a full MS/MS spectrum of the target peptide. The two most intense fragment ions (b or y fragment ions only) in the MS/MS spectrum for each acquired peptide were recorded by in-house developed software. The mass spectrometer collision energy (CE) was optimized for each transition with 5 different CE values automatically generated by in-house developed software. A solution containing all synthesized peptides at a concentration of 200 pmoL/mL was analyzed with the created MRM method. The two best peptides per proteins were selected to be monitored by the MRM assay.

The processed samples were resolubilized with 11 µL of a reconstitution solution containing 5 internal standard (IS) peptides each at 100 ng/mL. Eight (8) µL of material (~10 µg) was analyzed by LC/MRM-MS. Peptide separation was achieved using a BioBasic C18 column (Thermo) (320 µm x 150 mm, 5 µm particle size). The mobile phases were (A) 0.2% formic acid in water and (B) 0.2% formic acid in acetonitrile. Peptides were separated using a linear gradient (92.5% A to 60% A) for 21 min, followed by a wash at 60% B for 2 min. The flow rate was 10 µL/min. The transition peak areas were integrated using Elucidator software (Rosetta Biosciences) in combination with software developed at CellCarta for automated MRM peak integration.

Data processing and statistical analysis

For the analysis of the carbon fiber amperometry, the data was first standardized (mean=0 and variance=1). Data then was normalized by quantile method using *preprocessCore* R package. PCA analysis was performed using FactoMineR and factoextra R packages. Spearman's rank order correlation was performed using *cor* function from stats R package and plotted using corrplot and ggplot2 R packages. For comparison between paired Tumor (T) and Non-Tumor (NT) patients, paired Wilcoxon test was performed. For comparison between Tumor (T) patients, non-paired Wilcoxon test was performed.

For the differential expression analysis by mass spectrometry, the intensity values for all detected components were log (base e) transformed with values < 0 replaced by 0. Intensity data was normalized to account for small differences in protein concentration between samples. A subset of the samples was used to create a reference sample against which all samples were then normalized. The normalization factors were chosen so that the median of log ratios

between each sample and the reference sample over all the peptides was adjusted to zero. Intensities below Limit of Detection (LOD=100000) after normalization, were then linearly mapped to the range of (LOD/2, LOD) to avoid spurious large fold changes. Intensities above LOD were not changed. A two-way ANOVA model was used for the peptide level analysis and is defined as follows: $I_{ijk}=M+C_i+S_j+\varepsilon_{ijk}$ where I is the peptide intensity, M is the overall average intensity, C the 'clinical group' factor (matched non tumor and tumor), S the 'patient' factor that takes into consideration the 'pairing' nature of the data, and ε random error. FDR (False Discovery Rate) and q-value were calculated, based on the p-values obtained from the ANOVA model, using the Storey Tibshirani method to make multiple testing adjustments. Tukey's HSD (Honestly Significant Difference) method is used to perform post hoc contrast among different groups.

One protein may have several identified and quantified peptides. The following ANOVA model, which is an extension of the two-way ANOVA used above in the peptide level analysis, takes this into consideration by introducing a 'peptide factor' in the model: $I_{ijkl}=M+C_i+S_j+P_k+\varepsilon_{ijkl}$ where I is the protein intensity, M an overall constant, C the 'clinical group', S the 'patient' factor, and P the peptide factor. The number of the levels for P is protein-dependent, equal to the number of identified and quantified peptides for the protein.

For Multiple reaction monitoring (MRM) analysis, differential intensity (DI) ratios were calculated in pair wise comparisons for each transition as the median of the ratio of the normalized intensities of each group. Paired Student's t-test was applied for the expression analysis. Protein-level statistics were also computed by linearly combining the transitions of a given protein into a single variable and then applying a t-test.

All differential expression analysis and data visualization were done using R. PCA analysis was done using *prcomp* function from stats R package and plotted using ggplot2 R package. Volcano plot was performed using *EnhancedVolcano* function from R package.

Transcriptomic analyses

Gene expression data were retrieved from the GSE19422 dataset (https://www.ncbi.nlm.nih.gov/geo/query/acc.cgi?acc=GSE19422) (Lopez-Jimenez *et al.*, 2010) which includes 6 normal adrenal medulla and 61 Pheos. Consistently with the proteomic analysis, the 23 paraganglioma samples were not considered. The GSM483021 Pheo sample was excluded from our analysis because its transcriptomic profile, as revealed by clustering and UMAP analyses (data not shown), is similar to that of normal samples suggesting that it is misidentified. The expression level of each gene was calculated as the geometric mean of the significantly differentially expressed probes identified with the GEO2R web tool using a Benjamin-Hochberg FDR correction (q-values < 0.05). Genes of the regulated exocytosis (#BPGO:0045055) and secretory granule (#CCGO:0030141) GO terms were then selected for further analysis. Unsupervised hierarchical clustering was performed with Bioconductor (v.3.13) and R software (v.4.1.0) using Pearson correlation as distance calculation and complete linkage. The Fold change (FC) for each gene was calculated from the median expression values for the normal and Pheo groups and only those with a FC greater than or equal to 2 were retained for further analysis.

The correlation between the expression level of common genes and proteins was evaluated in both cytosolic and membrane fractions using Spearman correlation (GraphPad Prism v.8.1). In order to highlight functional clusters, an integrative analysis was conducted with Cytoscape software (v.3.8.2, (Shannon *et al.*, 2003)) using expression data and protein interaction data retrieved from STRING-DB (v.11.5, https://string-db.org/, (Szklarczyk *et al*, 2021)). An edge-weighted force directed layout has been applied to the interaction network. Gene/protein clusters were identified using the CytoCluster plugin for Cytoscape using the default settings except for minimum size: 6, minimum density: 0.25, Edge weights: Feature Distance, Node penalty:3.

Ethics approval and consent to participate

The present study used the data and the human biological material of the biological collection "Approche moléculaire des tumeurs corticosurrénaliennes" which was agreed by the "Comité de Protection des Personnes Est III" ethical advisory committee, and was conducted according to currently accepted ethical guidelines, including informed written consent approval signed by all patients prior to inclusion.

Funding and acknowledgements

This work was financially supported by ITMO Cancer AVIESAN (Alliance Nationale pour les Sciences de la Vie et de la Santé, National Alliance for Life Sciences & Health) within the framework of the Cancer Plan to SG and LB (Single Cell 2018 N° 19CS004-00); by the University of Strasbourg Institute for Advanced Study (USIAS) for a Fellowship, within the French national programme "Investment for the future" (IdEx-Unistra) to SG; by the Conseil Régional de Normandie to CD; by grants from the Agence Nationale pour la Recherche ("SecretoNET", N° ANR-16-CE17-0022-01) and from the Ligue contre le Cancer to SG (CCIR Grand-Est) and to CD (Comité Normand); by a fellowship from la Fondation pour la Recherche Médicale (FRM; FDM201806005916) to SM. INSERM is providing salary to SG and NV.

Conflict of interest

The authors declare that there is no conflict of interest that could be perceived as prejudicing the impartiality of the research reported.

References

Anantharam A, Kreutzberger AJB (2019) Unraveling the mechanisms of calcium-dependent secretion. *J Gen Physiol* 151: 417-434

Bader MF, Holz RW, Kumakura K, Vitale N (2002) Exocytosis: the chromaffin cell as a model system. *Ann N Y Acad Sci* 971: 178-183

Brown RL, Muzzafar T, Wollman R, Weiss RE (2006) A pituitary carcinoma secreting TSH and prolactin: a non-secreting adenoma gone awry. *Eur J Endocrinol* 154: 639-643

Burgoyne RD, Morgan A (2003) Secretory granule exocytosis. *Physiol Rev* 83: 581-632

Croise P, Houy S, Gand M, Lanoix J, Calco V, Toth P, Brunaud L, Lomazzi S, Paramithiotis E, Chelsky D *et al* (2016) Cdc42 and Rac1 activity is reduced in human pheochromocytoma and correlates with FARP1 and ARHGEF1 expression. *Endocr Relat Cancer* 23: 281-293

Cuttitta F, Carney DN, Mulshine J, Moody TW, Fedorko J, Fischler A, Minna JD (1985) Autocrine growth factors in human small cell lung cancer. *Cancer Surv* 4: 707-727

Daems T, Verhelst J, Michotte A, Abrams P, De Ridder D, Abs R (2009) Modification of hormonal secretion in clinically silent pituitary adenomas. *Pituitary* 12: 80-86

Desnos C, Schonn JS, Huet S, Tran VS, El-Amraoui A, Raposo G, Fanget I, Chapuis C, Menasche G, de Saint Basile G *et al* (2003) Rab27A and its effector MyRIP link secretory granules to F-actin and control their motion towards release sites. *J Cell Biol* 163: 559-570

Dineen R, Stewart PM, Sherlock M (2017) Acromegaly. *QJM* 110: 411-420

Eisenhofer G, Lenders JW, Goldstein DS, Mannelli M, Csako G, Walther MM, Brouwers FM, Pacak K (2005) Pheochromocytoma catecholamine phenotypes and prediction of tumor size and location by use of plasma free metanephrines. *Clin Chem* 51: 735-744

Fang Q, Berberian K, Gong LW, Hafez I, Sorensen JB, Lindau M (2008) The role of the C terminus of the SNARE protein SNAP-25 in fusion pore opening and a model for fusion pore mechanics. *Proc Natl Acad Sci U S A* 105: 15388-15392

Fathali H, Cans AS (2018) Amperometry methods for monitoring vesicular quantal size and regulation of exocytosis release. *Pflugers Arch* 470: 125-134

Gabel M, Delavoie F, Demais V, Royer C, Bailly Y, Vitale N, Bader MF, Chasserot-Golaz S (2015) Annexin A2-dependent actin bundling promotes secretory granule docking to the plasma membrane and exocytosis. *J Cell Biol* 210: 785-800

Gasman S, Vitale N (2017) Lipid remodelling in neuroendocrine secretion. *Biol Cell* 109: 381-390

Group NGSiPS, Toledo RA, Burnichon N, Cascon A, Benn DE, Bayley JP, Welander J, Tops CM, Firth H, Dwight T *et al* (2017) Consensus Statement on next-generation-sequencing-based diagnostic testing of hereditary phaeochromocytomas and paragangliomas. *Nat Rev Endocrinol* 13: 233-247

Guerin M, Guillemot J, Thouennon E, Pierre A, El-Yamani FZ, Montero-Hadjadje M, Dubessy C, Magoul R, Lihrmann I, Anouar Y *et al* (2010) Granins and their derived peptides in normal and tumoral chromaffin tissue: Implications for the diagnosis and prognosis of pheochromocytoma. *Regul Pept* 165: 21-29

Houy S, Estay-Ahumada C, Croise P, Calco V, Haeberle AM, Bailly Y, Billuart P, Vitale N, Bader MF, Ory S *et al* (2015) Oligophrenin-1 Connects Exocytotic Fusion to Compensatory Endocytosis in Neuroendocrine Cells. *J Neurosci* 35: 11045-11055

Juhlin CC, Skoglund S, Juntti-Berggren L, Karlberg M, Calissendorff J (2019) Non-functioning neuroendocrine pancreatic tumors transforming to malignant insulinomas - four cases and review of the literature. *Neuro Endocrinol Lett* 40: 175-183

Keshishian H, Addona T, Burgess M, Kuhn E, Carr SA (2007) Quantitative, multiplexed assays for low abundance proteins in plasma by targeted mass spectrometry and stable isotope dilution. *Mol Cell Proteomics* 6: 2212-2229

Lang T, Jahn R (2008) Core proteins of the secretory machinery. *Handb Exp Pharmacol*: 107-127

Lenders JW, Duh QY, Eisenhofer G, Gimenez-Roqueplo AP, Grebe SK, Murad MH, Naruse M, Pacak K, Young WF, Jr., Endocrine S (2014) Pheochromocytoma and paraganglioma: an endocrine society clinical practice guideline. *J Clin Endocrinol Metab* 99: 1915-1942

Lenders JWM, Kerstens MN, Amar L, Prejbisz A, Robledo M, Taieb D, Pacak K, Crona J, Zelinka T, Mannelli M *et al* (2020) Genetics, diagnosis, management and future directions of research of phaeochromocytoma and paraganglioma: a position statement and consensus of the Working Group on Endocrine Hypertension of the European Society of Hypertension. *J Hypertens* 38: 1443-1456

Lopez-Jimenez E, Gomez-Lopez G, Leandro-Garcia LJ, Munoz I, Schiavi F, Montero-Conde C, de Cubas AA, Ramires R, Landa I, Leskela S *et al* (2010) Research resource: Transcriptional profiling reveals different pseudohypoxic signatures in SDHB and VHL-related pheochromocytomas. *Mol Endocrinol* 24: 2382-2391

Malacombe M, Bader MF, Gasman S (2006) Exocytosis in neuroendocrine cells: new tasks for actin. *Biochim Biophys Acta* 1763: 1175-1183

Moog S, Houy S, Chevalier E, Ory S, Weryha G, Rame M, Klein M, Brunaud L, Gasman S, Cuny T (2018) 18F-FDOPA PET/CT Uptake Parameters Correlate with Catecholamine Secretion in Human Pheochromocytomas. *Neuroendocrinology* 107: 228-236

Mosharov EV, Sulzer D (2005) Analysis of exocytotic events recorded by amperometry. *Nat Methods* 2: 651-658

Onaitis MW, Kirshbom PM, Hayward TZ, Quayle FJ, Feldman JM, Seigler HF, Tyler DS (2000) Gastrointestinal carcinoids: characterization by site of origin and hormone production. *Ann Surg* 232: 549-556

Pappachan JM, Tun NN, Arunagirinathan G, Sodi R, Hanna FWF (2018) Pheochromocytomas and Hypertension. *Curr Hypertens Rep* 20: 3

Pourian M, Mostafazadeh DB, Soltani A (2015) Does this patient have pheochromocytoma? A systematic review of clinical signs and symptoms. *J Diabetes Metab Disord* 15: 11

Segura F, Brioso MA, Gomez JF, Machado JD, Borges R (2000) Automatic analysis for amperometrical recordings of exocytosis. *J Neurosci Methods* 103: 151-156

Shannon P, Markiel A, Ozier O, Baliga NS, Wang JT, Ramage D, Amin N, Schwikowski B, Ideker T (2003) Cytoscape: a software environment for integrated models of biomolecular interaction networks. *Genome Res* 13: 2498-2504

Song P, Sekhon HS, Jia Y, Keller JA, Blusztajn JK, Mark GP, Spindel ER (2003) Acetylcholine is synthesized by and acts as an autocrine growth factor for small cell lung carcinoma. *Cancer Res* 63: 214-221

Streit L, Moog S, Hugel S, Rame M, Tanguy E, Andry V, Schmid HA, Brunaud L, Bihain F, Nomine-Criqui C *et al* (2021) Somatostatin analogue pasireotide (SOM230) inhibits catecholamine secretion in human pheochromocytoma cells. *Cancer Lett*

Szklarczyk D, Gable AL, Nastou KC, Lyon D, Kirsch R, Pyysalo S, Doncheva NT, Legeay M, Fang T, Bork P *et al* (2021) The STRING database in 2021: customizable protein-protein networks, and functional characterization of user-uploaded gene/measurement sets. *Nucleic Acids Res* 49: D605-D612

Tanguy E, Coste de Bagneaux P, Kassas N, Ammar MR, Wang Q, Haeberle AM, Raherindratsara J, Fouillen L, Renard PY, Montero-Hadjadje M *et al* (2020) Mono- and Poly-unsaturated Phosphatidic Acid Regulate Distinct Steps of Regulated Exocytosis in Neuroendocrine Cells. *Cell Rep* 32: 108026

Tawfik B, Martins JS, Houy S, Imig C, Pinheiro PS, Wojcik SM, Brose N, Cooper BH, Sorensen JB (2021) Synaptotagmin-7 places dense-core vesicles at the cell membrane to promote Munc13-2- and Ca(2+)-dependent priming. *Elife* 10

Thompson LD (2002) Pheochromocytoma of the Adrenal gland Scaled Score (PASS) to separate benign from malignant neoplasms: a clinicopathologic and immunophenotypic study of 100 cases. *Am J Surg Pathol* 26: 551-566

Y-Hassan S, Falhammar H (2020) Cardiovascular Manifestations and Complications of Pheochromocytomas and Paragangliomas. *J Clin Med* 9

Zandee WT, Kamp K, van Adrichem RC, Feelders RA, de Herder WW (2017) Effect of hormone secretory syndromes on neuroendocrine tumor prognosis. *Endocr Relat Cancer* 24: R261-R274

Zhang R, Gupta D, Albert SG (2017) Pheochromocytoma as a reversible cause of cardiomyopathy: Analysis and review of the literature. *Int J Cardiol* 249: 319-323

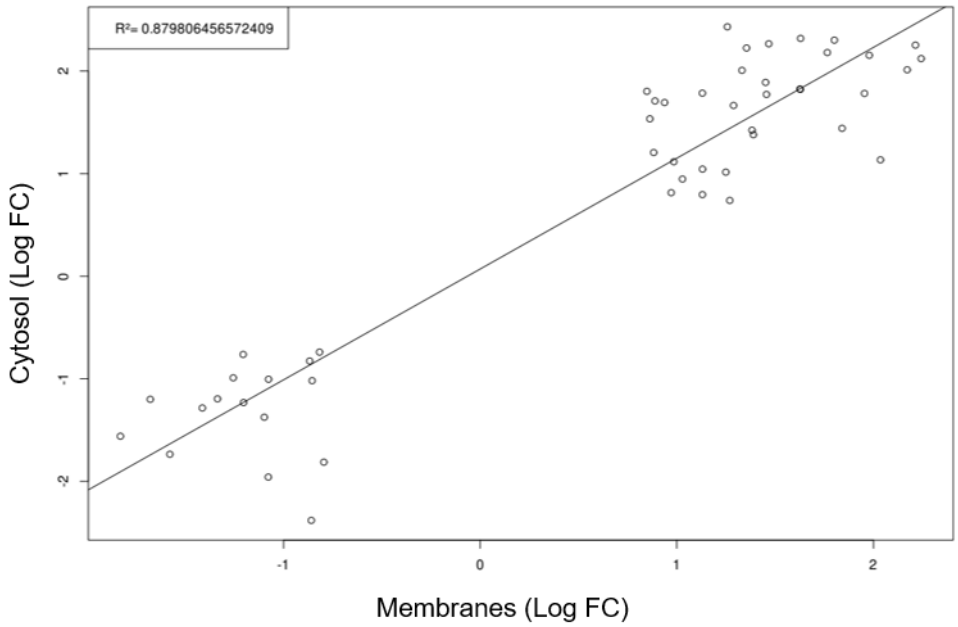

Supplementary Figure 1: Proteins found in common in the membrane and the cytosolic fractions vary in the same direction. *Among the 166 identified proteins whose expression significantly changes more than 2 fold, 50 are found in both cytosol- and membrane-enriched fractions. Linear regression analysis between the membrane-fold changes and the cytosolic-fold changes shows a positive correlation for both down-regulated and up-regulated proteins.*

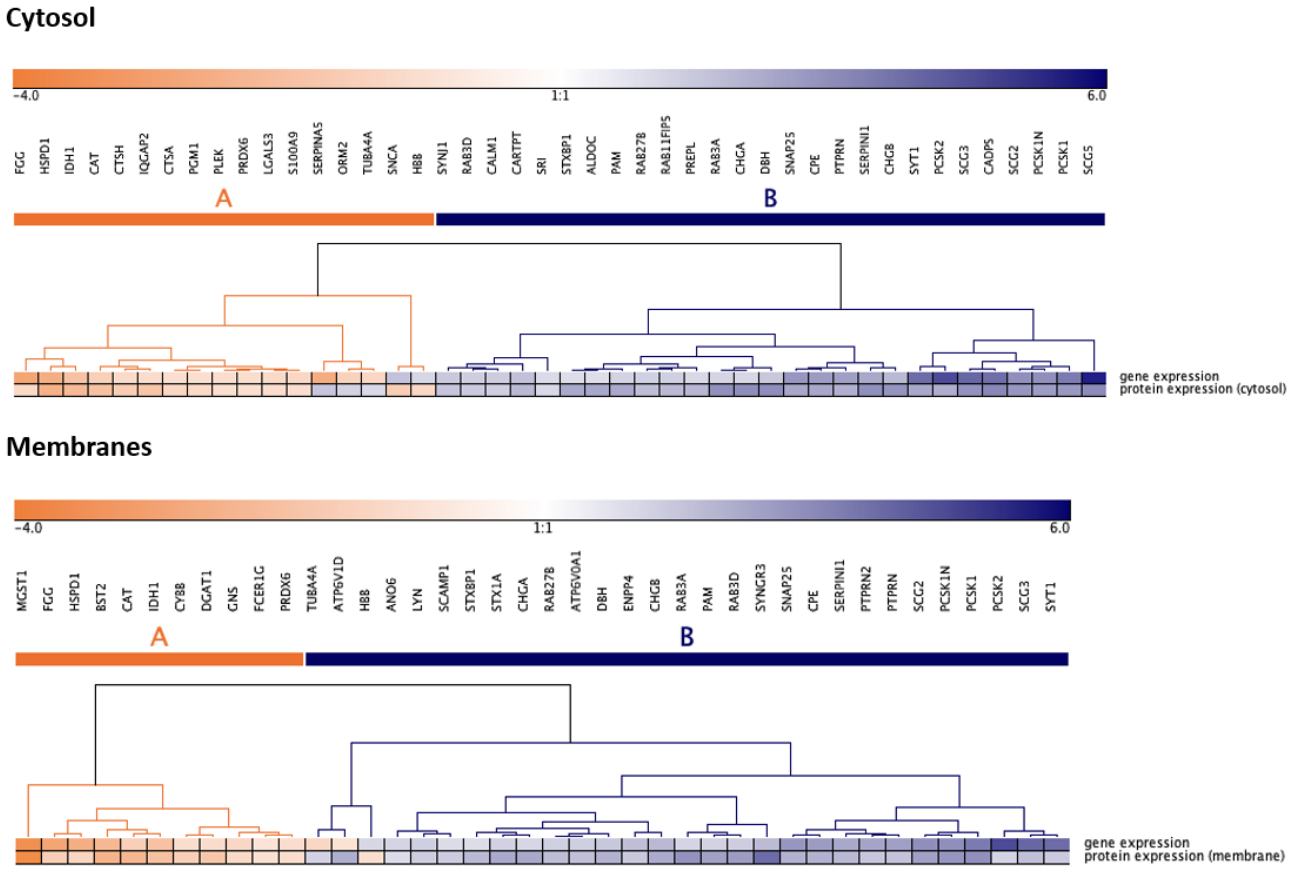

Supplementary Figure 2: Comparison of genes and proteins of the exocytic pathway deregulated in Pheo. *The 59 common differentially expressed genes (GSE19422) and proteins (this study) are selected from the exocytosis pathway. Unsupervised hierarchical clustering highlights two clusters of up- and down-regulated genes and proteins. Except for 5 (A) and 3 (B) genes/proteins, expression of all the genes (top row) and their proteins (bottom row) varies in the same direction. The color scale illustrates the over- (blue) or under- (red) expression of genes and proteins in Pheo compared to non-tumor tissue.*

Supplementary Table 1: Clinical, biochemical, and functional characteristics of the 27 patients with Pheo evaluated in this study.

#	Age	Gender	Symptom	Hormonal hypersecretion phenotype	Urinary MN (ULN ratio)	Urinary NMN (ULN ratio)	Plasma free MN (ULN ratio)	Plasma free NMN (ULN ratio)	Plasma CGA (ULN ratio)	Size (cm)	Ki-67 (%)	PASS score	Genetics
1	46	M	No	AD	8.1	1.2	-	-	4.9	3.7	-	3	Spor
2	54	F	No	AD	2.1	0.9	6.0	2.0	0.5	2	1	0	NF1
3	50	M	Yes	AD	2.8	13.5	3.1	2.0	1.5	3.5	-	1	NF1
4	34	M	Yes	NAD	0.6	7.1	1.0	3.0	4.8	1.7	4	1	SDHD
5	75	F	No	AD	14.1	4.7	-	-	4.6	8.0	-	3	Spor
6	61	M	Yes	NAD	1.5	2.0	2.0	10.0	-	2.5	-	3	Spor
7	64	M	No	AD	6.5	5.5	5.3	5.0	-	4.2	1	4	Spor
8	43	F	Yes	NAD	0.4	16	1.0	26.0	3.6	5.0	-	4	Spor
9	30	M	No	NAD	0.3	6.6	0.1	4.4	3.1	5.5	3	1	SDHB
10	47	M	Yes	NAD	1.0	8.7	-	-	-	4	-	2	-
11	47	F	Yes	AD	38.6	3.7	3.4	2.0	-	6.5	1	6	NF1
12	58	M	Yes	AD	1.9	4.6	-	-	0.9	4.4	5	0	-
13	36	F	Yes	AD	6.6	7.9	10.3	10	3.4	5.0	2	2	-
14	50	M	Yes	AD	18.0	5.2	-	-	-	7.0	1	2	Spor
15	42	M	Yes	NAD	2.0	13.0	0.1	5.6	1.5	4.0	-	0	-
16	47	F	Yes	NAD	4.6	23.4	-	-	1.2	7.0	1	0	Spor
17	58	F	Yes	AD	-	-	1.9	2.5	-	-	-	1	NF1
18	62	M	Yes	AD	54.1	9.6	-	-	-	4.5	-	0	-
19	46	M	Yes	NAD	0.9	12.5	0.8	8.3	10	5.0	-	3	RET
20	58	F	Yes	AD	2.8	10.3	4.4	7.4	-	3.5	1	4	-
21	53	F	No	AD	-	-	2.6	1.3	-	2.5	4	4	Spor
22	45	M	Yes	AD	-	-	19.9	2.2	-	4.9	1	1	Spor
1P	62	F	Yes	NAD	1.5	18.6	1.0	1.0	-	5	-	-	Spor
2P	48	F	Yes	AD	10	5	-	-	-	3.5	-	-	-
3P	58	M	Yes	AD	1.3	1.5	5.0	5.0	2.6	8.0	1	0	Spor
4P	52	F	Yes	AD					6.3	5.0	7	9	Spor
6P	69	M	Yes	AD	2.0	2.0	-	-	-	3.0	2	0	-

Age at diagnosis, gender (F: female, M: male), hormonal hypersecretion symptoms and phenotype, biochemical and functional values are represented for each patient number (#). AD: adrenergic, NAD: noradrenergic, MN: metanephrine, NMN: normetanephrine, ULN: upper limit normal, CGA: chromogranin A, PASS: Pheochromocytoma of the Adrenal Gland Scaled Score, Spor: sporadic, NF1: Neurofibromatosis type 1, RET: Rearranged during transfection, SDHB: Succinate dehydrogenase B, SDHD: Succinate dehydrogenase D, - : not available.

Supplementary Table 2: List of up- and down-regulated proteins in Pheo by comparison with the adjacent non-tumor tissue.

Gene	Protein	Entry (UniProtKB)	Fraction	Fold change	adj-p value	Function
SYNGR3	Synaptogyrin-3	O43761	Membrane	17.72	0.00018	Neurotransmiter uptake, regulation of dopamine transporter activity
MMRN1	Multimerin-1	Q13201	Cytosol	15.94	0.00016	Protein localized in granules, carrier protein for platelet factor V-Va
SERPINE2	Glia-derived nexin	P07093	Cytosol	11.29	0.00335	Secretory granule organization, granule biogenesis
CADPS	Calcium-dependent secretion activator 1	Q9ULU8	Cytosol	11.25	0.00016	Priming, calcium binding, plasma membrane binding, SNARE binding
SCG5	Neuroendocrine protein 7B2	P05408	Cytosol	10.59	0.00016	Secreted, in granules, peptide hormone processing
DBH	Dopamine beta-hydroxylase	P09172	Cytosol	10.09	0.00103	Dopamine synthesis pathway
CHGA	Chromogranin-A	P10645	Cytosol	9.92	0.00090	Granule biogenesis, secretory granule organization, peptide hormone processing
SERPINI1	Neuroserpin	Q99574	Cytosol	9.57	0.00103	Granule biogenesis, secretory granule organization, peptide hormone processing
RAB3A	Ras-related protein Rab-3A	P20336	Cytosol	9.45	0.00039	Vesicle trafficking, docking
PCSK1	Neuroendocrine convertase 1	P29120	Membrane	9.36	0.00050	Peptide hormone processing
SCG3	Secretogranin-3	Q8WXD2	Cytosol	9.19	0.00040	Secreted, in granules, peptide hormone processing
RAB3A	Ras-related protein Rab-3A	P20336	Membrane	9.09	0.00043	Vesicle trafficking, docking
CHGB	Secretogranin-1	P05060	Cytosol	8.79	0.00036	Granule biogenesis, secretory granule organization, peptide hormone processing
PCSK1N	ProSAAS	Q9UHG2	Membrane	8.72	0.00137	Peptide hormone processing
SCG2	Secretogranin-2	P13521	Cytosol	8.56	0.00034	Secreted, in granules, peptide hormone processing
PCSK1	Neuroendocrine convertase 1	P29120	Cytosol	8.29	0.00041	Peptide hormone processing
SV2B	Synaptic vesicle glycoprotein 2B	Q7L1I2	Membrane	7.90	0.00427	Binds synaptotagmin1, synaptotagmin trafficking, calcium regulator
RAB3D	Ras-related protein Rab-3D	O95716	Membrane	7.61	0.00059	Vesicle trafficking, docking
PCSK1N	ProSAAS	Q9UHG2	Cytosol	7.44	0.00087	Peptide hormone processing
GAL	Galanin peptides	P22466	Cytosol	7.39	0.00413	Inhibits exocytosis, peptide hormone processing
SCG2	Secretogranin-2	P13521	Membrane	7.19	0.00075	Secreted, in granules, peptide hormone processing
PAM	Peptidyl-glycine alpha-amidating monooxygenase	P19021	Membrane	7.02	0.00049	Secretory granule transmembrane protein, fatty acid biosynthetic process
PSAP	Prosaposin	P07602	Cytosol	6.63	0.00174	Lysosomal protein, lipid binding, GM1 binding
SYTL4	Synaptotagmin-like protein 4	Q96C24	Cytosol	6.58	0.00026	Priming, calcium binding, plasma membrane binding, SNARE binding
NAPB	Beta-soluble NSF attachment protein	Q9H115	Membrane	6.26	0.00050	Recycling, NSF activity, vesicular transport endosome golgi

SNAP25	Synaptosomal-associated protein 25	P60880	Cytosol	6.17	0.00089	SNARE, priming
CPE	Carboxypeptidase E	P16870	Cytosol	6.14	0.00145	Peptide hormone processing
ALDOC	Fructose-bisphosphate aldolase C	P09972	Cytosol	6.05	0.00090	Cytoskeletal binding protein, catalytic activity
TIMP1	Metalloproteinase inhibitor 1	P01033	Cytosol	6.03	0.00271	Metalloproteinase inhibitor, peptide hormone processing, secreted
CHGA	Chromogranin-A	P10645	Membrane	6.02	0.00381	Granule biogenesis, secretory granule organization, peptide hormone processing
SYT1	Synaptotagmin-1	P21579	Cytosol	5.93	0.00104	Priming, calcium binding, plasma membrane binding, SNARE binding
PAM	Peptidyl-glycine alpha-amidating monooxygenase	P19021	Cytosol	5.91	0.00051	Secretory granule transmembrane protein, fatty acid biosynthetic process
STX1A	Syntaxin-1A	Q16623	Membrane	5.88	0.00050	SNARE, priming
STXBP1	Syntaxin-binding protein 1	P61764	Cytosol	5.85	0.00034	Priming, fusion, binds SNARE and Munc13
CHGB	Secretogranin-1	P05060	Membrane	5.81	0.00077	Granule biogenesis, secretory granule organization, peptide hormone processing
ATP6AP2	Renin receptor	O75787	Membrane	5.80	0.00161	Renin receptor, V-ATPase assembly
ATP6V1D	V-type proton ATPase subunit D	Q9Y5K8	Membrane	5.50	0.00075	Vacuaolar ATPase activity
CTSZ	Cathepsin-Z	Q9UBR2	Cytosol	5.49	0.01285	Lysosomal protease (unclear role in exocytosis)
PCSK2	Neuroendocrine convertase 2	P16519	Cytosol	5.41	0.00578	Peptide hormone processing
B2M	Beta-2-microglobulin	P61769	Cytosol	5.33	0.00089	Peptide hormone processing, component of the major histocompatibility complex
CADPS2	Calcium-dependent secretion activator 2	Q86UW7	Cytosol	5.27	0.00041	Priming, calcium binding, plasma membrane binding, SNARE binding
PTPRN	Receptor-type tyrosine-protein phosphatase-like N	Q16849	Cytosol	5.26	0.00145	Regulates number of DCV, DCV maturation
PRCP	Lysosomal Pro-X carboxypeptidase	P42785	Cytosol	5.17	0.00290	Peptide hormone processing
DBH	Dopamine beta-hydroxylase	P09172	Membrane	5.08	0.00136	Dopamine synthesis pathway
CPE	Carboxypeptidase E	P16870	Membrane	5.07	0.00239	Peptide hormone processing
SNAP25	Synaptosomal-associated protein 25	P60880	Membrane	5.06	0.00076	SNARE, priming
RAPGEF4	Rap guanine nucleotide exchange factor 4	Q8WZA2	Cytosol	5.03	0.00115	Interacts with RIM2, cAMP dependent-PKA independant exocytosis, GEF of RAP 1-3
NFASC	Neurofascin	O94856	Membrane	4.85	0.00069	Adhesion, spectrin-organisation,plasma membrane localization
ECM1	Extracellular matrix protein 1	Q16610	Cytosol	4.70	0.00639	Platelet degranulation

RAB27A	Ras-related protein Rab-27A	P51159	Cytosol	4.62	0.00231	Interacts with granuphilin to regulate exocytosis, GTPase, docking, priming, DCV maturation, regulates endocytic pathway
CST3	Cystatin-C	P01034	Cytosol	4.58	0.00315	Neutrophil degranulation (unclear role in exocytosis)
SYT2	Synaptotagmin-2	Q8N9I0	Membrane	4.56	0.01268	Priming, calcium binding, plasma membrane binding, SNARE binding
CD44	CD44 antigen	P16070	Membrane	4.55	0.00066	Transmembrane protein, assembles via its cytoplasmic domain a protein complex including RhoA, Rac1, RHO-K and PLC, calcium mobilization, actin reorganization
PREPL	Prolyl endopeptidase-like	Q4J6C6	Cytosol	4.52	0.00075	PMSF regulation, synaptic vesicle exocytosis
SMPD1	Sphingomyelin phosphodiesterase	P17405	Cytosol	4.46	0.00089	Lipid reorganization of the plasma membrane, acid sphingomyelin phosphodiesterase activity
CD63	CD63 antigen	P08962	Membrane	4.41	0.00198	Reorganization of actin cytoskeleton, vesicular transport
RAB11FIP5	Rab11 family-interacting protein 5	Q9BXF6	Cytosol	4.34	0.00340	Protein trafficking from endosomes to plasma membrane, Rab effector, regulates V-ATPase
CARTPT	Cocaine- and amphetamine-regulated transcript protein	Q16568	Cytosol	4.33	0.00924	Regulates insulin secretion and production, no mechanism known
SERPINI1	Neuroserpin	Q99574	Membrane	4.32	0.00137	Granule biogenesis, secretory granule organization, peptide hormone processing
QPCT	Glutaminyl-peptide cyclotransferase	Q16769	Membrane	4.27	0.03997	Neutrophil degranulation (unclear role in exocytosis)
STXBP1	Syntaxin-binding protein 1	P61764	Membrane	4.27	0.00113	Priming, fusion, binds SNARE and Munc13
SYTL4	Synaptotagmin-like protein 4	Q96C24	Membrane	4.25	0.00095	Priming, calcium binding, plasma membrane binding, SNARE binding
NAPB	Beta-soluble NSF attachment protein	Q9H115	Cytosol	4.21	0.00194	Recycling, NSF activity, Vesicular transport endosome golgi
ATP8A1	Phospholipid-transporting ATPase IA	Q9Y2Q0	Membrane	4.20	0.00076	Lipid reorganization of the plasma membrane, flippase, P4-ATPase
RAB3B	Ras-related protein Rab-3B	P20337	Cytosol	4.13	0.01969	Vesicle trafficking, GTPase, vesicle biogenesis, priming
SYNGR1	Synaptogyrin-1	O43759	Membrane	4.02	0.00286	Synaptic vesicle protein, inhibits exocytosis
RAB27B	Ras-related protein Rab-27B	O00194	Membrane	4.00	0.00136	GTPase, docking, priming
RAB3B	Ras-related protein Rab-3B	P20337	Membrane	3.97	0.00233	Vesicle trafficking, GTPase, vesicle biogenesis, priming
RAB27B	Ras-related protein Rab-27B	O00194	Cytosol	3.96	0.00067	GTPase, docking, priming
SRP14	Signal recognition particle 14 kDa protein	P37108	Cytosol	3.92	0.00141	Secretory granule lumen (unclear role in exocytosis)
SYT7	Synaptotagmin-7	O43581	Membrane	3.88	0.00500	Priming, calcium binding, plasma membrane binding, SNARE binding

ATP6V0A1	V-type proton ATPase 116 kDa subunit a1	Q93050	Membrane	3.87	0.00135	Vacuaolar ATPase activity, vesicle acidification
SCG3	Secretogranin-3	Q8WXD2	Membrane	3.86	0.00331	Secreted, in granules, peptide hormone processing
GAL	Galanin peptides	P22466	Membrane	3.77	0.03071	Inhibits exocytosis, peptide hormone processing
PTPRN	Receptor-type tyrosine-protein phosphatase-like N	Q16849	Membrane	3.61	0.00305	Regulates number of DCV, DCV maturation
AMPD3	AMP deaminase 3	Q01432	Cytosol	3.59	0.00320	Energy metabolism (unclear role in exocytosis)
RAB4A	Ras-related protein Rab-4A	P20338	Cytosol	3.58	0.00149	Vesicle trafficking, docking, priming
DNM1L	Dynamin-1-like protein	O00429	Membrane	3.55	0.00137	GTPase, endocytosis, fusion
SERPINE2	Glia-derived nexin	P07093	Membrane	3.50	0.00662	Secretory granule organization, granule biogenesis
SYNJ1	Synaptojanin-1	O43426	Cytosol	3.49	0.00399	Regulation of lipid composition of the plasma membrane, endocytosis
TOLLIP	Toll-interacting protein	Q9H0E2	Membrane	3.47	0.00204	Autophagy, ubiquitin dependent process (unclear role in exocytosis)
PTPRN2	Receptor-type tyrosine-protein phosphatase N2	Q92932	Membrane	3.38	0.00137	Regulates number of DCV, DCV maturation, lipid reorganization
SERPINA5	Plasma serine protease inhibitor	P05154	Cytosol	3.36	0.01310	Secreted
PFN2	Profilin-2	P35080	Cytosol	3.33	0.00163	Actin reorganization, binds PIP2, Inhibits PIP2 hydrolysis
ENPP4	Bis(5'-adenosyl)-triphosphatase ENPP4	Q9Y6X5	Membrane	3.24	0.00449	Unclear role in exocytosis
ALDOA	Fructose-bisphosphate aldolase A	P04075	Cytosol	3.22	0.00584	Glycogenesis, scaffold protein, secreted
TUBB4B	Tubulin beta-4B chain	P68371	Membrane	3.16	0.00164	Microtubules component, cytoskeletal protein
RAB3D	Ras-related protein Rab-3D	O95716	Cytosol	3.10	0.00301	Vesicle trafficking, docking, priming
DYNC1H1	Cytoplasmic dynein 1 heavy chain 1	Q14204	Membrane	3.09	0.00201	Vesicle transporter, ATPase
TUBB	Tubulin beta chain	P07437	Membrane	3.09	0.00243	Microtubules component, cytoskeletal protein
SYT1	Synaptotagmin-1	P21579	Membrane	3.08	0.00386	Priming, calcium binding, plasma membrane binding, SNARE binding
SCAMP1	Secretory carrier-associated membrane protein 1	O15126	Membrane	3.08	0.00388	Present at docking, priming sites, role in exocytosis
DYNC1LI1	Cytoplasmic dynein 1 light intermediate chain 1	Q9Y6G9	Membrane	3.07	0.00220	Vesicle transporter, ATPase
APP	Amyloid-beta precursor protein	P05067	Cytosol	3.04	0.00251	Interacts with synaptic release machinery, facilitate transmitters release
TOM1	Target of Myb protein 1	O60784	Cytosol	2.98	0.00293	Priming, negatively regulates exocytosis
CD9	CD9 antigen	P21926	Membrane	2.95	0.00831	Cell adhesion, Fusion

RPH3A	Rabphilin-3A	Q9Y2J0	Membrane	2.93	0.03797	Docking, fusion, priming
PPP3CB	Serine/threonine-protein phosphatase 2B catalytic subunit beta isoform	P16298	Cytosol	2.87	0.00228	Protein phosphatase (unclear role in exocytosis)
LYN	Tyrosine-protein kinase Lyn	P07948	Membrane	2.87	0.00386	Tyrosine protein kinase (unclear role in exocytosis)
DYNC1H1	Cytoplasmic dynein 1 light intermediate chain 1	Q9Y6G9	Cytosol	2.83	0.00233	Vesicle transporter, ATPase
CALM1	Calmodulin-1	P0DP23	Cytosol	2.82	0.00301	Priming, fusion, vesicle trafficking
VAMP3	Vesicle-associated membrane protein 3	Q15836	Membrane	2.80	0.00332	SNARE, involved in vesicular transport from late endosomes to TGN
SDF4	45 kDa calcium-binding protein	Q9BRK5	Membrane	2.79	0.01404	Involved in exocytosis of zymogens by pancreatic acini
MYO5A	Unconventional myosin-Va	Q9Y4I1	Membrane	2.76	0.00731	Actin motor, vesicle transport, cytoskeleton
TOLLIP	Toll-interacting protein	Q9H0E2	Cytosol	2.75	0.00446	Autophagy, ubiquitin dependent process (unclear role in exocytosis)
SNAPIN	SNARE-associated protein Snapin	O95295	Cytosol	2.72	0.00307	Vesicle trafficking, priming, fusion, interacts with SNAREs
APP	Amyloid-beta precursor protein	P05067	Membrane	2.67	0.00311	Interacts with synaptic release machinery, facilitate transmitters release
GARS	Glycine--tRNA ligase	P41250	Cytosol	2.65	0.00332	Unclear role in exocytosis
TUBA4A	Tubulin alpha-4A chain	P68366	Membrane	2.63	0.01056	Microtubules component, cytoskeletal protein
CLU	Clusterin	P10909	Membrane	2.61	0.00736	Secreted
ORM2	Alpha-1-acid glycoprotein 2	P19652	Cytosol	2.58	0.00440	Lipid reorganization, actin reorganization, endocytosis
SDF4	45 kDa calcium-binding protein	Q9BRK5	Cytosol	2.57	0.00877	Involved in exocytosis of zymogens by pancreatic acini
PCSK2	Neuroendocrine convertase 2	P16519	Membrane	2.55	0.02773	Peptide hormone processing
FAM3C	Protein FAM3C	Q92520	Membrane	2.52	0.01201	Interacts with SNAP23 and RalA (unclear role in exocytosis)
SERPINF2	Alpha-2-antiplasmin	P08697	Cytosol	2.48	0.00378	Secretory granule organization, granule biogenesis
DBNL	Drebrin-like protein	Q9UJU6	Membrane	2.48	0.00462	Binds actin and dynamin-1, actin polymerization, endocytosis
CTSZ	Cathepsin-Z	Q9UBR2	Membrane	2.43	0.01022	Lysosomal protease (unclear role in exocytosis)
DNAJC3	DnaJ homolog subfamily C member 3	Q13217	Membrane	2.41	0.00880	Unclear role in exocytosis
PFN2	Profilin-2	P35080	Membrane	2.41	0.00569	Actin reorganization, binds PIP2, Inhibits PIP2 hydrolysis
VAT1	Synaptic vesicle membrane protein VAT-1 homolog	Q99536	Cytosol	2.37	0.01795	Vesicle protein, calcium binding (unclear role in exocytosis)
RAB27A	Ras-related protein Rab-27A	P51159	Membrane	2.36	0.01470	Interacts with granuphilin to regulate exocytosis, GTPase, docking, priming, DCV maturation, regulates endocytic pathway

RAB3GAP1	Rab3 GTPase-activating protein catalytic subunit	Q15042	Cytosol	2.36	0.01642	Vesicle trafficking, docking
PFKL	ATP-dependent 6-phosphofructokinase, liver type	P17858	Cytosol	2.33	0.01501	Unclear role in exocytosis
TIMP1	Metalloproteinase inhibitor 1	P01033	Membrane	2.33	0.04521	Metalloproteinase inhibitor, peptide hormone processing, secreted
SRI	Sorcin	P30626	Cytosol	2.29	0.01565	Calcium binding protein, lipid rafts
SEPT5	Septin-5	Q99719	Cytosol	2.27	0.00802	GTPase, cytoskeleton reorganization
LGALS3BP	Galectin-3-binding protein	Q08380	Cytosol	2.25	0.01028	Unclear role in exocytosis
TUBA4A	Tubulin alpha-4A chain	P68366	Cytosol	2.25	0.02017	Microtubules component, cytoskeletal protein
MIF	Macrophage migration inhibitory factor	P14174	Cytosol	2.24	0.02151	Cytokin, secreted
TUBB	Tubulin beta chain	P07437	Cytosol	2.21	0.01572	Microtubules component, cytoskeletal protein
ENDOD1	Endonuclease domain-containing 1 protein	O94919	Membrane	2.20	0.01953	Unclear role in exocytosis
PNP	Purine nucleoside phosphorylase	P00491	Cytosol	2.20	0.01009	Unclear role in exocytosis, maybe secreted
ACTR1B	Beta-centractin	P42025	Membrane	2.17	0.01056	Cytoskeletal organization, microtubules
ANO6	Anoctamin-6	Q4KMQ2	Membrane	2.17	0.01947	Phospholipid scrambling, lipid reorganization of the plasma membrane
TRAPPC1	Trafficking protein particle complex subunit 1	Q9Y5R8	Cytosol	2.16	0.04291	Vesicular transport ER to Golgi
AP2A2	AP-2 complex subunit alpha-2	O94973	Membrane	2.10	0.01217	Endocytosis, protein transport
DNM1L	Dynamin-1-like protein	O00429	Cytosol	2.09	0.01299	GTPase, endocytosis, fusion
MAN2B1	Lysosomal alpha-mannosidase	O00754	Cytosol	2.01	0.01332	Unclear role in exocytosis
A2M	Alpha-2-macroglobulin	P01023	Cytosol	-2.03	0.01478	Unclear role in exocytosis
STXBP3	Syntaxin-binding protein 3	O00186	Membrane	-2.06	0.01323	Docking, fusion, priming
APRT	Adenine phosphoribosyltransferase	P07741	Cytosol	-2.06	0.01507	Unclear role in exocytosis
DERA	Deoxyribose-phosphate aldolase	Q9Y315	Membrane	-2.07	0.02014	Unclear role in exocytosis
VAPA	Vesicle-associated membrane protein-associated protein A	Q9P0L0	Membrane	-2.08	0.02654	Vesicle trafficking
FGA	Fibrinogen alpha chain	P02671	Cytosol	-2.09	0.03711	Unclear role in exocytosis
PTGES2	Prostaglandin E synthase 2	Q9H7Z7	Cytosol	-2.14	0.00915	Receptor coupled to G proteine Gi, AMPc (unclear role in exocytosis)
VCL	Vinculin	P18206	Cytosol	-2.15	0.01566	Actin filament binding protein, cytoskeletal reorganization

THBS1	Thrombospondin-1	P07996	Cytosol	-2.16	0.02546	Secreted
SCCPDH	Saccharopine dehydrogenase-like oxidoreductase	Q8NBX0	Membrane	-2.21	0.01198	Unclear role in exocytosis
ANXA2	Annexin A2	P07355	Membrane	-2.23	0.02400	Calcium binding protein, lipid binding, cytoskeletal reorganization, lipid microdomains
FCER1G	High affinity immunoglobulin epsilon receptor subunit gamma	P30273	Membrane	-2.23	0.00763	Unclear role in exocytosis
FGA	Fibrinogen alpha chain	P02671	Membrane	-2.26	0.02179	Unclear role in exocytosis
PRDX6	Peroxiredoxin-6	P30041	Cytosol	-2.28	0.00786	Phospholipase, phospholipids reorganization, secreted
PLEK	Pleckstrin	P08567	Cytosol	-2.29	0.03768	PKC target, phosphoinositide binding, lipid binding
HBB	Hemoglobin subunit beta	P68871	Membrane	-2.34	0.01042	Unclear role in exocytosis
S100A9	Protein S100-A9	P06702	Cytosol	-2.35	0.00924	Calcium and zinc binding, degranulation neurtrophil by MAPK dependent mechanism, modulation microtubule cytoskeleton, secreted
PROS1	Vitamin K-dependent protein S	P07225	Membrane	-2.36	0.03700	Calcium binding (unclear role in exocytosis)
SLIRP	SRA stem-loop-interacting RNA-binding protein, mitochondrial	Q9GZT3	Cytosol	-2.37	0.02528	Unclear role in exocytosis
PRDX6	Peroxiredoxin-6	P30041	Membrane	-2.37	0.00880	Phospholipase, phospholipids reorganization, secreted
LGALS3	Galectin-3	P17931	Cytosol	-2.40	0.01781	Unclear role in exocytosis
NIT2	Omega-amidase NIT2	Q9NQR4	Cytosol	-2.43	0.00548	Secreted (unclear role in exocytosis)
ELANE	Neutrophil elastase	P08246	Membrane	-2.43	0.02242	Secreted (unclear role in exocytosis)
CYBA	Cytochrome b-245 light chain	P13498	Membrane	-2.48	0.02766	Unclear role in exocytosis
STOM	Stomatin	P27105	Membrane	-2.52	0.00533	Lipid raft component, scaffold protein
RNPEP	Aminopeptidase B	Q9H4A4	Cytosol	-2.54	0.00389	Peptidase (unclear role in exocytosis)
GLA	Alpha-galactosidase A	P06280	Cytosol	-2.59	0.03945	Glycosphyngolipid hydrolisis, lipid reorganization, lipid degradation in lysosome, glycoprotein
S100A13	Protein S100-A13	Q99584	Membrane	-2.60	0.04494	Calcium binding, binds phosphatidylserine, lipid binding, secreted, regulate FGF-1 secretion
PGM1	Phosphoglucomutase-1	P36871	Cytosol	-2.64	0.00315	Glucose synthesis and catalysis pathway, secreted
LAMTOR1	Ragulator complex protein LAMTOR1	Q6IAA8	Cytosol	-2.65	0.00603	mTor pathway, activated by amino-acids, anchoring regulator complex to membranes, may play a role in RhoA activation, lysosomal exocytosis

GNS	N-acetylglucosamine-6-sulfatase	P15586	Membrane	-2.67	0.03261	Calcium binding (unclear role in exocytosis)
FGG	Fibrinogen gamma chain	P02679	Cytosol	-2.69	0.01811	Unclear role in exocytosis
FGB	Fibrinogen beta chain	P02675	Cytosol	-2.72	0.02085	Unclear role in exocytosis
CTSA	Lysosomal protective protein	P10619	Cytosol	-2.73	0.04395	Lysosomal protease (unclear role in exocytosis)
HBB	Hemoglobin subunit beta	P68871	Cytosol	-2.76	0.00349	Unclear role in exocytosis
METTL7A	Methyltransferase-like protein 7A	Q9H8H3	Membrane	-2.82	0.01175	Unclear role in exocytosis
APOOL	MICOS complex subunit MIC27	Q6UXV4	Membrane	-2.85	0.01445	Mitochondrial inner membrane (unclear role in exocytosis)
DLD	Dihydrolipoyl dehydrogenase, mitochondrial	P09622	Cytosol	-2.87	0.00574	Unclear role in exocytosis
FGB	Fibrinogen beta chain	P02675	Membrane	-2.93	0.01206	Unclear role in exocytosis
HSPD1	60 kDa heat shock protein, mitochondrial	P10809	Membrane	-2.93	0.00580	Protein folding, acrosomal exocytosis
ACAA1	3-ketoacyl-CoA thiolase, peroxisomal	P09110	Membrane	-2.99	0.00305	Lipid metabolism, fatty acid metabolism, insulin secretion
STX7	Syntaxin-7	O15400	Cytosol	-3.10	0.00905	Protein trafficking from plasma membrane to endosomes, homotypic fusion of endocytic organelles, endocytosis, SNARE, SNARE binding,
ITGA2B	Integrin alpha-IIb	P08514	Membrane	-3.17	0.00290	Platelet degranulation
CTSD	Cathepsin-D	P07339	Membrane	-3.17	0.02030	Lysosomal protease (unclear role in exocytosis)
COMMD3	COMM domain-containing protein 3	Q9UBI1	Cytosol	-3.19	0.00751	Phosphoinositides regulation, lipids
F13A1	Coagulation factor XIII A chain	P00488	Cytosol	-3.29	0.01539	Calcium binding, coagulation factor (unclear role in exocytosis)
PPBP	Platelet basic protein	P02775	Cytosol	-3.31	0.00348	Stimulates formation and secretion of plasminogen activator, secreted
GLB1	Beta-galactosidase	P16278	Membrane	-3.32	0.01990	Lipid organisation and metabolism
PTGES2	Prostaglandin E synthase 2	Q9H7Z7	Membrane	-3.33	0.00219	Receptor coupled to G proteine Gi, AMPc (unclear role in exocytosis)
ANXA11	Annexin A11	P50995	Membrane	-3.35	0.00743	Vesicular trafficking ER to golgi, calcium binding, lipid binding
SYPL1	Synaptophysin-like protein 1	Q16563	Membrane	-3.36	0.00318	Syntaxin1 binding, SNARE binding, VAMP2 binding, endocytosis
CYBB	Cytochrome b-245 heavy chain	P04839	Membrane	-3.40	0.00825	Regulation of cellular pH, ROS (unclear role in exocytosis)
GLB1	Beta-galactosidase	P16278	Cytosol	-3.42	0.00759	Lipid organisation and metabolism
FN1	Fibronectin	P02751	Membrane	-3.42	0.00157	Cell adhesion, cell motility, opsonization, wound healing, maintenance of cell shape, extracellular matrix glycoprotein (unclear role in exocytosis)
FGG	Fibrinogen gamma chain	P02679	Membrane	-3.50	0.00445	Unclear role in exocytosis

SNCA	Alpha-synuclein	P37840	Cytosol	-3.54	0.00338	Synaptic vesicle trafficking, priming, fusion, dilation of fusion pores, calcium regulation, SNAREs assembly
FLNA	Filamin-A	P21333	Cytosol	-3.60	0.00118	Actin filament branching, cytoskeletal regulation, scaffold protein, exocyst
CTSH	Pro-cathepsin H	P09668	Cytosol	-3.62	0.00312	Lysosomal protease (unclear role in exocytosis)
CREG1	Protein CREG1	O75629	Cytosol	-3.63	0.00275	Control of cell growth and differenciation, secreted
F13A1	Coagulation factor XIII A chain	P00488	Membrane	-3.79	0.00168	Calcium binding, coagulation factor (unclear role in exocytosis)
ACAA1	3-ketoacyl-CoA thiolase, peroxisomal	P09110	Cytosol	-3.94	0.00584	Lipid metabolism, fatty acid metabolism, insulin secretion
FLNA	Filamin-A	P21333	Membrane	-4.09	0.00175	Actin filament branching, cytoskeletal regulation, scaffold protein, exocyst
DGAT1	Diacylglycerol O-acyltransferase 1	O75907	Membrane	-4.26	0.00164	Triacylglycerol synthesis, DAG pathway, lipid organization
IQGAP2	Ras GTPase-activating-like protein IQGAP2	Q13576	Cytosol	-4.37	0.00163	Binds to activated Cdc42 and Rac1, associate with calmodulin, cytoskeleton regulation, exocyst complex, endocytosis
CD109	CD109 antigen	Q6YHK3	Cytosol	-4.64	0.00175	Modulates negatively TGFB1 signaling in keratinocytes (unclear role in exocytosis)
CAT	Catalase	P04040	Cytosol	-4.74	0.00053	Antioxidant enzyme (unclear role in exocytosis)
IDH1	Isocitrate deshydrogenase	O75874	Membrane	-4.82	0.00136	Catalytic activity, phospholipid biosynthetic and catalytic process, insulin secretion
FERMT3	Fermitin family homolog 3	Q86UX7	Cytosol	-5.00	0.00064	Cell adhesion (unclear role in exocytosis)
CYB5R3	NADH-cytochrome b5 reductase 3	P00387	Cytosol	-5.02	0.00051	Lipid organisation, cholesterol biosynthesis (unclear role in exocytosis)
PPBP	Platelet basic protein	P02775	Membrane	-5.33	0.00136	Stimulates formation and secretion of plasminogen activator, secreted
IDH1	Isocitrate deshydrogenase	O75874	Cytosol	-5.64	0.00051	Catalytic activity, phospholipid biosynthetic and catalytic process, insulin secretion
SCCPDH	Saccharopine dehydrogenase-like oxidoreductase	Q8NBX0	Cytosol	-6.09	0.00034	Unclear role in exocytosis
CAT	Catalase	P04040	Membrane	-6.20	0.00049	Antioxidant enzyme (unclear role in exocytosis)
BST2	Bone marrow stromal antigen 2	Q10589	Membrane	-6.81	0.00050	Actin cytoskeleton organization
HSPD1	60 kDa heat shock protein, mitochondrial	P10809	Cytosol	-7.05	0.00060	Protein folding, acrosomal exocytosis
COL1A1	Collagen alpha-1(I) chain	P02452	Membrane	-9.00	0.00050	Extracellular matrix (unclear role in exocytosis)
PROS1	Vitamin K-dependent protein S	P07225	Cytosol	-10.73	0.00266	Calcium binding (unclear role in exocytosis)

MGST1	Microsomal glutathione S-transferase 1	P10620	Membrane	-23.19	0.00018	Unclear role in exocytosis

List of proteins involved in exocytosis detected by mass spectrometry in cytosol- and membrane-enriched fractions. The median value of the fold change is obtained by comparing the expression from 5 pairs of tumor matched to non-tumor tissues. DAG: diacylglycerol, DCV: dense-core vesicle, ER: endoplasmic reticulum, FGF-1: fibroblast growth factor 1, GM1: monosialotetrahexosylganglioside, MAPK: mitogen-activated protein kinase, NSF: N-ethylmaleimide-Sensitive Factor, PKC: protein kinase C, PLC: phospholipase C, SNARE: soluble N-ethylmaleimide sensitive factor attachment receptor, ROS: reactive oxygen species, TGFB1: transforming growth factor beta 1, TGN: trans-Golgi network.